

Electrical Conductivity and Wettability Evaluation of Thin PEDOT: PSS films
Printed via Electrically Assisted Direct Ink Deposition with Ultrasonic Vibration for
Perovskite Solar Cells

by

Rohan Ravishekar

A Thesis Presented in Partial Fulfillment
of the Requirements for the Degree
Master of Science

Approved April 2023 by the
Graduate Thesis Committee:

Xiangjia Li, Chair
Terry Alford, Co-Chair
Gokul Pathikonda

ARIZONA STATE UNIVERSITY

May 2023

ABSTRACT

Direct Ink Deposition is a type of 3D printing that utilizes a nozzle to coat thin films onto substrates. Electro spray deposition is a subcategory of Direct Ink Deposition wherein a very strong electric field is applied between the nozzle exit and the substrate, which results in the precursor polymer ink to be sprayed onto the substrate in the form of micro- or nano-droplets. As of today, its applications are limited to producing small area polymer solar cells or for biomedical applications, particularly in laboratories, but in the future, with optimization of electro spray deposition, this method can be further expanded to 3D printing components that can be used in the aerospace, automotive, and other such large-scale industries. The objective of this research is to see how application of ultrasonic vibrations during, and post deposition affects the morphology, electrical conductivity, and the respective surface properties of the thin Poly(3,4 – Ethylenedioxythiophene)-Poly(Styrenesulfonate) (PEDOT:PSS) film printed via electro spray deposition. The printing setup was previously designed and constructed, wherein the syringe was loaded with the PEDOT:PSS and Isopropyl Alcohol (IPA) solution which was then printed onto thin and small sized Indium Tin Oxide (ITO) substrates under the application of a high voltage. The distance of the nozzle from the substrate was appropriately adjusted via the vertical linear movable stage before printing, as well as the voltage supply. Deposition time was set using an Arduino code that controlled the horizontal movement of the shutter attached to the bottom of the vertical linear aluminum frame. Horizontally and vertically induced vibrations were turned on during and post deposition to analyze

the effect of both on the films' properties through an ultrasonic transducer. The electrical sheet resistance of the PEDOT:PSS films was measured using a 4-point probe device and the surface contact angle of water on the PEDOT:PSS was measured using a contact angle meter. From the results obtained, it was concluded that the application ultrasonic vibrations improved wettability compared to the films printed without any vibrations. Furthermore, the electrical sheet resistance and contact angle of pure ITO was measured as a reference.

ACKNOWLEDGEMENTS

I would like to sincerely express my heartfelt gratitude to Dr. Xiangjia (Cindy) Li, my faculty advisor, for providing me with unwavering support and guidance throughout the duration of my master's thesis. Thank you for giving me the opportunity to be a research aide in the Lab of Manufacturing Innovation over the last two academic semesters, aiding me in quenching my thirst for knowledge and giving me the right opportunities to gain a huge amount of research experience. I would also like to express my profound gratitude to my faculty co-chair Dr. Terry Alford for providing me the opportunity to conduct my research in their lab space and committee member Dr. Gokul Pathikonda for their time and consideration to be a part of my thesis committee.

I would also like to thank my lab partner and current doctoral student Yizhen Zhu for their assistance whenever I needed it, as well as Tengteng Tang, who helped me with certain aspects of my research. Additional gratitude towards Banashree Gogoi, current doctoral student under Dr. Terry Alford for her advice, and Carson Gockley, current undergraduate honors student, for his time and patience, and for initially teaching me how to go about executing the experimental procedure which was used for my thesis research.

Furthermore, I would like to thank the Eyring Materials Center, located in the Goldwater Center for Science and Engineering, as well as Physical Science Building – Wing B, for allowing us to use their equipment for my research. Thank you to Xan Hendersen, who mentored me on how to use the KLA Tencor

Omnimapper 4-point probe located at Macro Technology Works at ASU Research Park. I express my sincere gratitude to ASU Macro Technology Works for allowing me to use their equipment.

Finally, I would like to thank my family and friends for their unconditional support, love, and encouragement throughout my time at Arizona State University as a master's student in aerospace engineering. Thank you to my lab mates, colleagues, mentors, advisors, and professors for their assistance over the two academic years of my master's degree.

TABLE OF CONTENTS

	Page
LIST OF TABLES	viii
LIST OF FIGURES	ix
LIST OF EQUATIONS.....	xii
CHAPTER	
1. INTRODUCTION	1
1.1 Background	1
1.2 Motivation and Objectives.....	3
2. LITERATURE REVIEW	6
2.1 Current Manufacturing Processes of PEDOT:PSS Solid Films	8
2.1.1 Spray Coating	8
2.1.2 Spin Coating	11
2.1.3 Slot-Die Coating.....	13
2.1.4 Drop Casting.....	16
2.2 3D Printing of PEDOT:PSS	19
2.3 Challenges.....	20
2.4 Principle and Methodology	22
3. EXPERIMENTAL PROCEDURE	26
3.1 Materials Selection	26
3.2 PEDOT:PSS Printing Ink Preparation.....	26

CHAPTER	Page
3.3 Electrically Assisted Direct Ink Deposition With and Without Vibration.....	28
3.3.1 Electrically Assisted Direct Ink Deposition	28
3.3.2 Electrically Assisted Direct Ink Deposition With Ultrasonic Vibration	29
3.3.3 Ultrasonic Vibrations after Electrically Assisted Direct Ink Deposition	30
3.4 Post Deposition Heat-Treatment	31
3.5 Electrical Conductivity.....	32
3.6 Wettability	34
4. RESULTS AND DISCUSSION.....	37
4.1 Ultrasonic Vibration Module Construction.....	37
4.1.1 Horizontal Vibration Module.....	37
4.1.1 Vertical Vibration Module.....	38
4.2 Control of Ultrasonic Vibrations	39
4.2.1 Connection of Ultrasonic Transducer.....	39
4.2.2 Vibration Regulation	40
4.2.3 Potential Influence of Ultrasonic Vibrations	43
4.2.3.1 Horizontal	43
4.2.3.2 Vertical.....	44
4.3 Electrical Conductivity.....	45
4.3.1 0.15 A Horizontal Vibrations	45

CHAPTER	Page
4.3.2 0.26 A Horizontal Vibrations	47
4.3.3 0.15 A Vertical Vibrations	48
4.3.4 0.26 A Vertical Vibrations	49
4.4 Wettability Evaluation	51
4.4.1 0.15 A Horizontal Vibrations	51
4.4.2 0.26 A Horizontal Vibrations	52
4.4.3 0.15 A Vertical Vibrations	54
4.4.4 0.26 A Vertical Vibrations	55
5. CONCLUSION AND FUTURE WORK.....	58
5.1 Summary	58
5.2 Future Work.....	59
REFERENCES	61

LIST OF TABLES

Table	Page
1. Intervals of Applied Ultrasonic Vibrations and their Significance	39
2. Parameters of Printing and their Meaning	41
3. Sheet Resistance of Films Printed With 0.15A of Horizontal Vibrations.....	46
4. Sheet Resistance of Films Printed With 0.26A of Horizontal Vibrations.....	48
5. Sheet Resistance of Films Printed With 0.15A of Vertical Vibrations.....	49
6. Sheet Resistance of Films Printed With 0.26A of Vertical Vibrations.....	50
7. Contact Angle of Films Printed With 0.15A Horizontal Vibrations	52
8. Contact Angle of Films Printed With 0.26A of Horizontal Vibrations	53
9. Contact Angle of Films Printed With 0.15A of Vertical Vibrations	55
10. Contact Angle of Films Printed With 0.26A of Vertical Vibrations	56

LIST OF FIGURES

Figure	Page
1. Perovskite Solar Cell Structure ^[40]	3
2. Ultrasonication Effect on Vibrating Thin Films ^[60]	7
3. Induced Air Flow over Vibrating Thin Films ^[60]	8
4. Spray Coating of PEDOT:PSS onto Substrates ^[41]	9
5. Spin Coating of Solutions Showing all 4 Stages ^[42]	13
6. Slot-Die Coating (a) Concept and Design, (b) Perovskite Solar Cell Structure ^[43]	16
7. Drop Casting Method ^[44]	19
8. Electro spray Deposition Technique, With Magnification of Taylor Cone and Jet Stream.....	20
9. (i) Natural dripping, (ii) Micro-dripping, (iii) Unstable jet cone, (iv) Stable Jet Cone, (v) Multi-Jet Cone Modes of E-Spray Under Varying Applied Voltage ^[18]	23
10. Taylor Cone Formation and Jet Stream Ejection Under Influence of Electric Field	24
11. Printing Setup With (a) Horizontal Vibration Module, (b) Vertical Vibration Module.....	25
12. Prepared PEDOT:PSS Solution. (10% PEDOT in 90% IPA v/v).....	27
13. (a) ITO Slides Held In Place Using Stainless Steel Clamps, (b) Isometric View of CAD Generated Clamp, (c) Side-Isometric View of CAD Generated Clamp.....	28

Figure	Page
14. Arduino Control Board With Ultrasonic Vibrations Generator Relay.....	30
15. Printed ITO Slides Kept For Annealing on ALT VWR Ceramic Stirrer.....	32
16. Four-Point Probe Schematic and Working ^[45]	33
17. KLA Tencor Omnimapper 4-Point Probe Device at MTW	34
18. Contact Angle Meter ^[59]	36
19. Rendered Model of Printing Setup With Horizontally Induced Ultrasonic Vibrations	37
20. Rendered Model of Printing Setup With Vertically Induced Ultrasonic Vibrations.....	38
21. Connection of Transducer, Wave Generator and Relay	40
22. Vibration Control Via Relay	43
23. Potential Influence of Ultrasonic Vibrations on the PEDOT:PSS Nanofilm	45
24. Sheet Resistance of Films Printed With 0.15A of Horizontal Ultrasonic Vibrations.....	46
25. Sheet Resistance of Films Printed With 0.26A of Horizontal Ultrasonic Vibrations.....	47
26. Sheet Resistance of Films Printed With 0.15A of Vertical Ultrasonic Vibrations.....	48
27. Sheet Resistance of Films Printed With 0.26A of Vertical Ultrasonic Vibrations.....	49
28. Contact Angle of Films Printed With 0.15A of Horizontal Ultrasonic Vibrations.....	51

Figure	Page
29. Contact Angle of Film With (a) No Vibrations and (b) 0.15A, 15/15s Horizontal Vibrations.....	52
30. Contact Angle of Films Printed With 0.26A of Horizontal Ultrasonic Vibrations.....	53
31. Contact Angle of Film With (a) No vibrations and (b) 0.26A, 1.5/1.5s Horizontal Vibrations.....	54
32. Contact Angle of Films Printed With 0.15A of Vertical Ultrasonic Vibrations.....	54
33. Contact Angle of Film With (a) No Vibrations and (b) 0.15A, 5/5s Vertical Vibrations.....	55
34. Contact Angle of Films Printed With 0.26A of Vertical Ultrasonic Vibrations.....	56
35. Contact Angle of Film With (a) No Vibrations and (b) 0.26A, 5/5s Vertical Vibrations.....	57

LIST OF EQUATIONS

Equation	Page
1. Goldschmidt Tolerance Factor.....	3
2. Deposition Thickness for Non-Vibrating Nanofilms	6
3. Deposition Diameter for Non-Vibrating Nanofilms.....	6
4. Seebeck Coefficient for Conducting Polymers	17
5. Droplet Size Equation by De La Mora and Loscertales.....	23
6. Droplet Evaporation Time using Square Law.....	24
7. Electrical Conductivity of Thin Films	33
8. Young's Contact Angle	34
9. Marangoni Velocity Equation	35

CHAPTER 1 INTRODUCTION

1.1 Background

In recent years, flexible optoelectronic devices such as perovskite solar cells (PSCs) have gained a lot of research attention due to properties such as broad absorption spectrum, high charge mobility, low cost and solution-processable fabrication. In a really short span, the energy conversion efficiency of perovskite solar cells has jumped from 3.8% to 25.2% [6]. Progression in this field will play a significant role in improving the quality of next generation displays that can be manufactured via economic roll-to-roll processes that are lightweight and have a high degree of mechanical flexibility [5]. In general, PSCs have either a mesoporous or a planar heterojunction configuration. In the mesoporous heterojunction configuration for perovskite solar cells, a metal-oxide-nanoparticle scaffold is used as a support for the perovskite (light-absorber) layer. In order to incorporate this in a PSC, a high temperature sintering process is needed and has been realized as one of the root causes of hysteresis in current–voltage characteristics. These challenges can be mitigated by utilizing the inverted planar heterojunction configuration, where the perovskite layer is sandwiched between a hole transport layer (HTL) and the electron transport layer (ETL) [14]. PEDOT: PSS, which is an electro-conductive polymer solution, has been widely used as the hole transport layer (HTL) in organic solar cell devices because of its high transparency in the visible region, good thermal stability, high mechanical stability, strong hole affinity and high work function [2]. In the most commonly seen structure of the perovskite solar cell, solution processed electron donor materials (P3HT) and

electron acceptor materials (PCBM) are used to their complete potential to fabricate these devices. Besides this, the HTL (PEDOT:PSS) and ETL (MAPbX₃, X = Cl, Br, I), low work function metals such as Ca/Al are used as an electron-blocking layer and electron accepting electrode respectively. However, these metals are not very stable at room temperature, which is why substitutes such as Au/Ag are more frequently used as the hole collecting electrodes, which increases the overall cost of the perovskite solar cell. [17] Perovskite solar cells are defined on the basis of the crystal structure of light absorbing materials with the formula ABX₃, where A and B are cations with coordinate numbers 12 and 8, respectively, and X is the anion [26]. A lot of research has been conducted on improving the interface between the hole and electron transport layers in PSCs since charge transport and recombination is a critical deciding factor for overall PCEs of such devices [27].

At present, a lot of experiments are seen to make use of spin-coating to synthesize PSCs due to its simplicity and ease of access. In this method, the perovskite precursor solution is directly deposited via a nozzle onto a substrate that is spun at a certain rate, and the droplet(s) spread along the surface of the substrate due to shear forces [28]. One of the primary challenges in making use of the spin-coating method to fabricate PSCs is the utilization of antisolvents for smooth films and morphology. Common antisolvents include toluene and chlorobenzene, which are not easily available commercially, and are quite expensive [29]. Coming to the creation of the perovskite compound, one can incorporate a somewhat broad spectrum of elements having different valencies at

the respective cationic and anionic sites, given that charge neutrality is conserved. This is also one of the reasons that perovskite is widely used in the fabrication of organic photovoltaic cells. The formability of different types of the perovskite compound is calculated using a dimensionless number called the Goldschmidt tolerance factor (t), which indicates crystal stability and structure deformity. This factor is given by ^[30],

$$t = \frac{1}{\sqrt{2}} \frac{(r_A + r_X)}{(r_M + r_X)} \quad (1) \quad [30]$$

where r_A is the radius of the cation A, r_M is the radius of the cation B, and r_X is the radius of the anion. For a perovskite compound containing a transition metal cation and an oxide anion, a cubic crystal structure is obtained when $t = 1$, and an octahedral structure is formed for $t < 1$ ^[30].

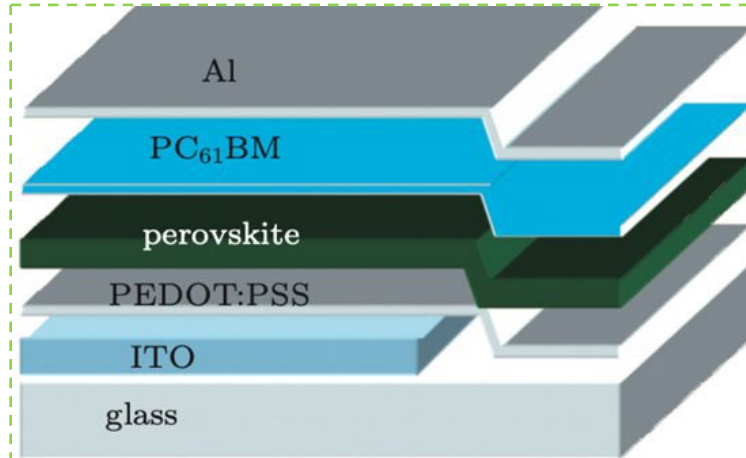


Fig.1 Perovskite solar cell structure ^[40].

1.2 Motivation and Objectives

The electro-spray or e-spray technique has been introduced recently since it is compatible with manufacturing of organic solar cells (OSCs). This method eliminates the high-pressure atomizing gas that is used in handheld spray.

Moreover, this technique does not require a directing carrier gas utilized in the ultrasonic spray, because the charged mists move about searching for a potential surface to land on that is opposite in charge to their own, enabling high deposition efficiency without a heated substrate. Since e-spray can work without the use of gas-induced evaporation, the drying time of the deposited film can be regulated by independently adjusting either the substrate temperature, the amount of high boiling-point additives, or both ^[15]. Y. Kim et al. ^[15] studied and analyzed the properties of the highly conductive PEDOT:PSS (CLEVIOS™ PH1000) that was e-sprayed onto substrates by individually varying the experiment's parameters such as substrate temperature, solvent dilution ratio, and amount of DMSO added. The optimized electrical conductivity of the electro sprayed film was found to be comparable to spin-coated films with a value of 800 S cm⁻¹. Additionally, the film had no macroscopic morphological boundaries or electrical point defects. Furthermore, Y. Tajima et al. ^[22] fabricated a thin film OLED organic photovoltaic cell device via electro spray deposition (ESD) and found that the films' morphology and its performance was comparable to conventional spin-coated methods. H. Lee et al. ^[23] fabricated an OPV device with ESD PEDOT:PSS as the HTL, but spin-coated HAT-CN (1,4,5,8,9,11-hexaazatriphenylene hexacarbonitrile) which was incorporated between the PEDOT:PSS and PCBM layers to improve overall PCE of the OPV device. In accordance with their results, they found out that the PCE of non HAT-CN containing OPV devices have a PCE of 0.52%, while the HAT-CN containing device had an enhanced PCE of about 0.83%. Kavadiya et al. ^[31-32] optimized a two-step synthesis process for electro spraying perovskite film and this

resulted in an overall device PCE of 12%. Prior to this study, all PSCs were manufactured by spin-coating entirely or excluding the perovskite film, which was electrospayed. Y. Jiang et al. ^[32] for the first time, fabricated an all electro-spray printed PSC which had a PCE of 15%, the highest achievable efficiency till that time. M. Hameed et al. ^[33] used a hybrid e-sprayed electron transport material (ZnO nanofibers + TiO₂ beads) in their PSCs to obtain a PCE of 20.27%.

CHAPTER 2 LITERATURE REVIEW

PEDOT:PSS is a solution-processed solar cell material and can be deposited on a substrate using a casting method, such as dip coating, doctor blading, slot-die coating, ink-jet printing, spray coating, and spin coating using inexpensive equipment and under ambient atmospheric conditions. The cost of an all-solution-processed device is thereby substantially reduced [4]. In a PEDOT:PSS dispersion, the polymeric chains are more probable to arrange themselves into a random coil conformation. When such a dispersion is coated onto a substrate, a thin film is created with grains containing doped conjugated polymer coils. [19] T.C. Wei et al. [20] summarized that the pristine PEDOT:PSS film initially exhibited weak phase separation between the PEDOT coiled chains and PSS molecules, where the grains that consisted of PEDOT chains were randomly oriented in the PSS matrix. This led to fewer charge transport pathways, resulting in low electrical conductivity. However, addition of ethylene glycol (EG) as a co-solvent during solution preparation led to a screening effect that decreased the Coulombic interaction between the cationic PEDOT chains and anionic PSS molecules. This was due to the high dielectric constant of EG.

Y.Zhu et al. [16] derived the following two expressions for deposition thickness and diameter for nanofilms printed without any vibrations using the electrically assisted direct ink deposition method,

$$t_d = 4\gamma t / \pi D^2 \quad (2) \quad [16]$$

$$D = 0.1794H \quad (3) \quad [16]$$

where D is the deposition diameter, H is the height of the nozzle from the substrate, t is the deposition time, γ is the flow rate of the ink through the nozzle exit, and t_d is the deposition thickness. [16]

Ultrasonic vibrations can be produced by speakers or piezoelectric transducers. It is known to have improved film area coverage, integrity, and uniformity due to better coalesce and spreading of impinging droplets before complete drying. Due to ultrasonic atomization effect, the impinging droplets break up into smaller droplets and spread evenly across the surface of the substrate. Fig.2 shows the effect of ultrasonic vibrations on a thin TiO_2 /Graphene-flake film, wherein the vibrations break the TiO_2 gel-network on one hand, excites, homogenizes, and mixes the film on the other. [60]

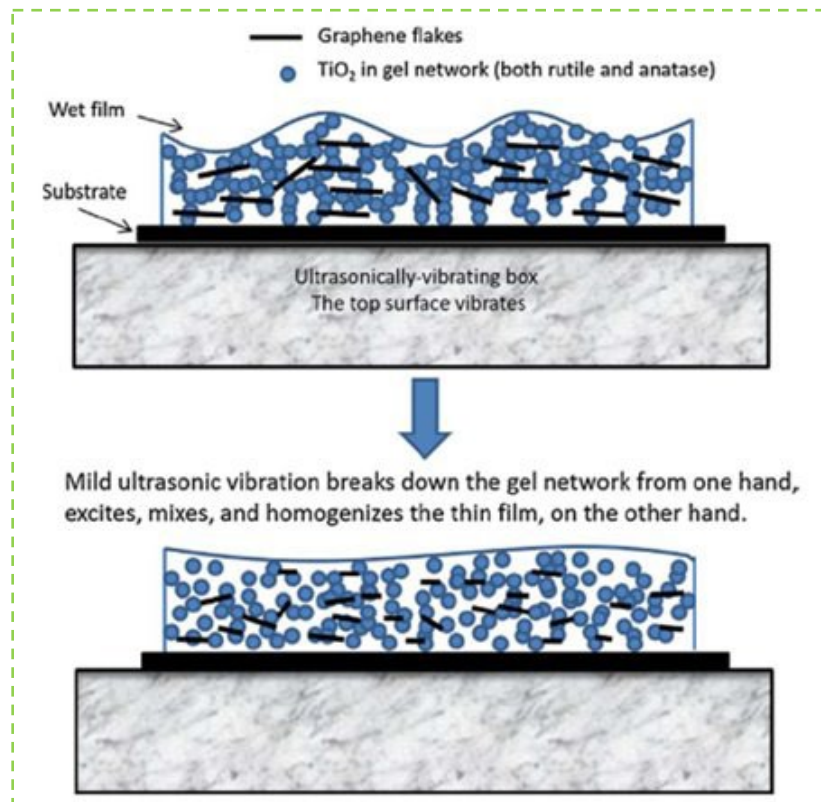


Fig.2 Ultrasonication effect on vibrating thin films. [60]

Fig.3 shows the induced air flow over thin films with applied ultrasonic vibrations. In the case of horizontal vibrations, micro-vortices are induced all over the thin film's surface, enhancing the circulation of heat, resulting in more uniform heat transfer and better morphology of the thin film post deposition. However, in the case of vertical vibrations, there comes the existence of stagnation points along the thin film surface, resulting in uneven heating and evaporation of the solvents in the film, resulting in a relatively more non-uniform film compared to the case of horizontally applied ultrasonic vibrations. That being said, it is to be noted that both horizontally and vertically applied ultrasonic vibrations will improve the film's morphology compared to films printed without any vibrations due to the ultrasonic atomization effect as mentioned previously in this literature. [60]

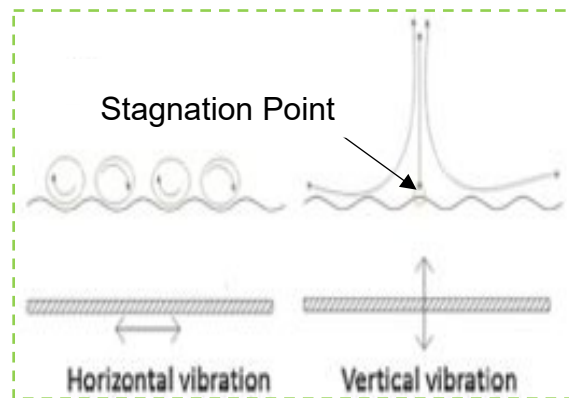


Fig.3 Induced air flow over vibrating thin films. [60]

2.1 Current manufacturing processes of PEDOT:PSS solid films

2.1.1 Spray Coating

Sustainable development of organic solar cell technology entails the application of scalable techniques, such as spray coating for fast, roll-to-roll, and low-cost fabrications of such solution-processed layers. Spray coating consists of atomization of a precursor solution, partial evaporation of flying droplets, droplet

impact on the substrate, dynamic spreading and wetting, droplet coalescence, film formation, and drying. Spray coating, amongst other scalable methods mentioned above, is more suitable for the fabrication of ultrathin films, required for some particular applications in which a nano-scale film thickness is essential for effective charge separation and transfer, for instance, in a thin-film organic solar cell. Single or multiple deposition layers may be applied depending on the process and substrate characteristics and film thickness and roughness requirements [4]. F.M. Kordshuli et al. [3] studied the effect of addition of IPA and graphene on the morphology of the PEDOT:PSS films made using conventional spray coating (no substrate vibrations imposed). From their observations, they showed that addition of IPA to PEDOT:PSS solution results in an increase in electrical conductivity; however, the film becomes less uniform and surface defects increase, as substantiated by a considerable increase in surface roughness when IPA is added. The increase in conductivity as a result of addition of IPA to the PEDOT:PSS solution may be due to the excess charges created by the organic solvent.

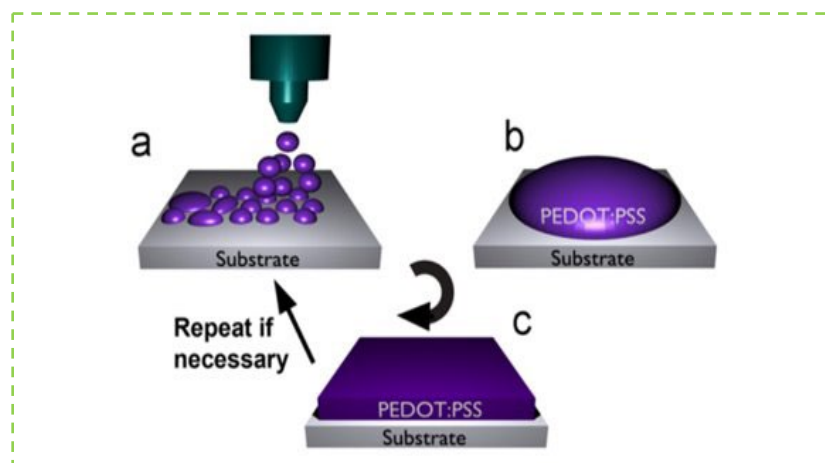


Fig.4 Spray coating of PEDOT:PSS onto substrates [41].

Furthermore, addition of highly conductive graphene dopants into PEDOT:PSS + IPA causes further enhancement in conductivity and an improvement in the film intactness and mechanical strength. The dispersed graphene sheets could act as a bridge or interlinking lattice in the thin film, improving the surface and inner structure of the film. It was also proven that the introduction of graphene to pristine PEDOT:PSS causes a 10x increase in the conductivity. This is because of the significantly high conductivity of graphene. PEDOT:PSS can be dispersed with water and spin-coated to generate highly conductive transparent films, with conductivities between 0.05-10 S cm⁻¹ and low sheet resistance [19]. F. Gong et al. [46] fabricated a multifunctional polymer fabric via spray-coating PEDOT:PSS solutions in 5 wt% DMSO. The resulting material exhibited a high conductivity, with a minimum sheet resistance of 12.10 Ω sq⁻¹. This enhancement of electrical conductivity can be attributed to improved uniformity, thickness of the film, and emergence of PEDOT:PSS microcrystals in the multilayered coating, thereby meaning better conduction pathways. Sheet resistance of the pure graphene film was found to be around 700 Ω sq⁻¹, and the surface roughness was very high due to presence of impurities. By adding PEDOT:PSS/DIW/DMSO to the graphene film in a 4:5:0.5 volume ratio, the sheet resistance of the thin film was decreased to 500 Ω sq⁻¹. [47]

Moreover, the most optimal morphology and electrical conductivity was observed at a 4:6:0.5 volume ratio of PEDOT:PSS/DIW/DMSO. The sheet resistance of this film came out to be as low as 320 Ω sq⁻¹ [47]. It was found that the surface roughness of the spray coated PEDOT:PSS films was majorly decreased

with imposed ultrasonic vibrations by comparing AFM images of no-vibrations and applied ultrasonic vibrations. In both cases, there were absence of pinholes, but however, the no-vibration case film had deeper valleys and higher peaks, which makes the film more susceptible to damage and rupture, thereby decreasing the overall efficiency and performance of the perovskite solar cell. Moreover, the average thickness of the films printed with ultrasonic vibration were lower ^[48]. E-J. Bae et al. ^[49] produced Te-based heterostructures coated with PEDOT:PSS to be spray coated onto substrates to create thermoelectric generators. The power factor was optimized to $60.05 \mu\text{W m}^{-1} \text{K}^{-2}$, with an electrical conductivity of 69.99 S cm^{-1} .

2.1.2 Spin Coating

Spin coating is a process that has been commonly used to manufacture integrated circuits, optical mirrors, flexible optoelectronics, and organic solar cells. The pioneering analysis of spin coating was performed more than fifty years ago taking into account the spreading of a thin axisymmetric film of Newtonian fluid on a planar substrate rotating with constant angular velocity. In many cases the coating material is polymeric and is applied in the form of a solution from which the solvent evaporates. Centrifugal force drives the fluid radially outward, and the film flattens out due to evaporation and surface tension. ^[7]

Spin coating has the following key stages - fluid dispense, spin-up, stable fluid flow, and evaporation dominated drying. For most of the process, stages 3 and 4 dominate over the first two. However, at an engineering level, the viscous flow effects dominate early on while the evaporation processes dominate later ^[7].

Due to surface tensions, PEDOT:PSS solution is difficult to spin directly on glass because of adhesion and wettability issues. Spin coating is relatively easier to execute with an addition of 5 % IPA to the PEDOT:PSS solution. Spin coating produces uniform layers with thickness ranging from 50 nm up to several hundreds of nanometers depending on spin coater rotation speed [8]. T. Cheng et al. [1] made use of spin coating to fabricate multiple layers of doped PEDOT:PSS solution in high-performance free-standing PEDOT:PSS electrodes with increased optoelectronic performance, high flexibility, smooth morphology, and excellent electrochemical performance. The influence of the doping surfactant on the performance of the PEDOT:PSS electrodes, including morphology, optoelectronic performance, and the electrochemical performance, was meticulously investigated. It was found that 2% (vol/vol) surfactant can not only enhance the electrical conductivity but also improve the electrochemical performance of the PEDOT:PSS electrodes.

Flexible and transparent all-solid-state supercapacitors with both superior electrochemical performance and relatively high optical transparency using the resultant high performance PEDOT:PSS films as both the current collectors and the active electrodes were fabricated for the first time. [1] According to F.-Z. Hui et al. [50], when the PEDOT:PSS film was spin-coated onto substrates under an electric field of strength 6 kV cm^{-1} , the device exhibits an open-circuit voltage of 0.563 V, a fill factor (FF) of 0.245, and a PCE of 2.93%. However, the film becomes more rough as compared to zero applied electric field - it was increased from 0.86 nm to 1.01 nm for these PEDOT:PSS films. The hybrid spray-coated

PEDOT:PSS/CNT electrodes showed much lower sheet resistance compared to pure CNT electrodes since the PEDOT:PSS nanoparticles filled up the voids between the nanotubes of CNTs, hence creating a conduction pathway for electron transfer, eventually reducing the tube-tube junction resistance. These hybrid electrodes also exhibited enhanced flexibility [51]. The surface roughness of the pure ITO film was 2.43 nm and decreased by almost 50% when spin coated with PEDOT:PSS film to 1.23 nm. However, the roughness increases when the annealing temperature of the substrate with PEDOT reaches 200 °C, and then drops with further increase in temperature due to film degradation. With a heat treatment time of 50 min, the conductivity of the spin-coated films increases by 27% to approximately 3800 S cm⁻¹ [52].

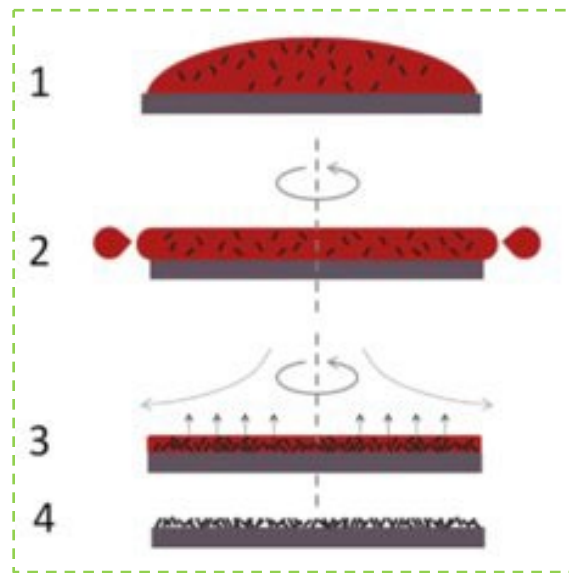


Fig.5 Spin-coating of solutions showing all 4 stages [42].

2.1.3. Slot-Die Coating

Among various scalable coating techniques, slot-die coating is one of the attractive techniques due to its potential coating uniformity across large areas, high

throughput with the ability to coat at speeds greater than 600 m min^{-1} , high material utilization with little waste, as well as the ability to be integrated into both sheet-to-sheet (S2S) and roll-to-roll coating (R2R) systems. In addition, the film thickness can be controlled by varying the precursor concentration, solution precursor feed rate, gap height, and coating speed ^[10]. Due to the fact that slot-die coating is a pre-metered process, it is much more efficient in printing composites onto substrates as compared to spray coating and spin coating. In a typical slot-die coating process, the coating head is placed very close to and across the substrate. The ink is then pumped or fed into the coating head via a syringe pump, with the ink being forced out of the narrow slit along the length of the head ^[9].

The slot-die coating process could be a promising process for industrial use and solution-processed PSCs due to its advantages such as a continuous process, compatibility, high throughput, unlimited substrate size, and ease control of film uniformity and thickness ^[12]. L.Tzounis et al. ^[12] made use of the slot-die coating technique to obtain almost pinhole-free perovskite films using lead acetates instead of lead halides (PbI_3 or PbCl_3) via a one-step process and shorted annealing time (a few minutes). The perovskite layer characterization yielded the same features as initially spin coated fabricated devices that have shown a PCE of 9.4 %. The morphology of the printed films was studied using SEM images. It was observed that the film was uniformly covered over the entire thickness with fine grains, which is considered ideal to collect maximum charge across the film thickness. Furthermore, the top view SEM images indicate that the slot-die coated film was compact with minimum pinholes. The average grain size was found to be

about 1.5 μm which was found to be comparable to that prepared by spin coating with the same precursor ink. This thereby proved that using slot-die coating is much more efficient than processes like spray or spin coating, due to the fact that the very similar film properties were obtained with less wastage of precursor inks. The success or failure of fine stripe coatings was affected by the surface morphology of the slot-die head and its effect was more pronounced with increasing number of stripes (μ -tips). Fine strips of average width 168 μm were printed using 150 μm wide slot-die tips, whereas the thickness of the films was 103 nm under a print speed of 20 mm s^{-1} [53].

A.W. Parsekian et al. [54] printed PEDOT:PSS parallel stripes onto flexible polyethylene terephthalate (PET) substrates using slot-die coating method with the absence of wettability enhancing dopants. These strips had a width ranging from 400 to 850 μm , displaying an electrical conductivity of about 1.5 S cm^{-1} , which is almost 7 times that of pure PEDOT:PSS organic polymer. It was found that the thickness and morphology of the slot-die coated films were extremely sensitive to the coating parameters such as substrate temperature, slot-die coating speed, and ink flow rates. After careful optimization of these parameters, it was possible to obtain the PEDOT:PSS layer (HIL) with an optimal thickness of 34 ± 3 nm and the F8:F8BT layer (EML) with a thickness of 66 ± 5 nm. The OLEDs fabricated from these films have shown uniform light emission with a low turn-on voltage of 3.5 V, a maximum current efficiency of 1.7 cd A^{-1} , and a brightness of 357 cd m^{-2} at 10 V. The OLED performances thus indicate that slot-die coating is an efficient and

feasible technique to fabricate PEDOT:PSS and F8:F8BT layers to be used in such devices [55].

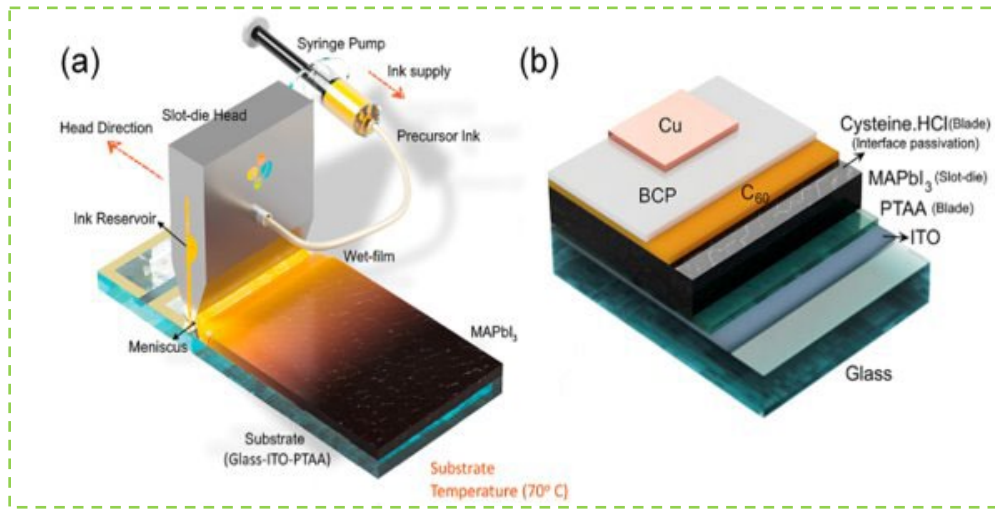


Fig.6 Slot-die coating (a) concept and design, (b) perovskite solar cell structure [43].

2.1.4 Drop-Casting

Recently, mixtures of PEDOT and polystyrenesulfonate (PSS) have been found to have large electrical conductivity in the in-plane direction when drop-cast from aqueous suspensions in combination with high boiling-point cosolvents such as dimethyl sulfoxide (DMSO), making PEDOT:PSS a promising candidate for applications in thermoelectric energy conversion [13]. Q. Meng et al. [11] prepared PC-Te/PEDOT:PSS composite films by drop-casting method. It was shown that the electrical conductivity of the composite films radically increases after being treated with H_2SO_4 whereas the extent of improvement decreases with increase in PC-Te concentration. The Seebeck coefficient is the voltage produced in a material with a known and present temperature difference and is related to the entropy of charge carriers in the material. The Seebeck coefficient was calculated by the slope of the linear relationship between the thermal electromotive force and the

temperature difference (~5–15 K) between two ends on one side of each sample. The Seebeck coefficient of the composite films monotonously increases with increasing PC-Te concentration due to the large Seebeck coefficient of PC-Te nanorods (139 $\mu\text{V K}^{-1}$). Consequently, the maximum power factor of the pristine composite film is 51.6 $\mu\text{W m}^{-1}\text{K}^{-2}$, which is higher than that of each individual component of the composite films. However, the Seebeck coefficient decreases after the composite films have been treated with H_2SO_4 . The maximum power factor of 141.9 $\mu\text{W m}^{-1}\text{K}^{-2}$ is obtained for the sample $\text{P}_{12}\text{-PC-Te}_{90}$ composite film, which is 2.75 times as high as that of the pristine films (51.6 $\mu\text{W}/\text{mK}^2$). For conducting polymers, the Seebeck Coefficient is given by the following equation -

$$S = \kappa_B(E - E_F)/e\kappa_B T \quad (4) \quad [11]$$

where S is the Seebeck Coefficient, κ_B is the Boltzmann Constant, e is the charge of the electron (1.6×10^{-19} eV), T is the absolute temperature (in K), E is the total energy of the localized states, and E_F is the energy of the Fermi level. From their analysis and calculations, J. Liu et al. [13] concluded that addition of DMSO as a cosolvent majorly increases the in-plane electrical conductivity σ . It was also observed that the increase in σ with DMSO exhibited different trends. In the drop-cast films, σ increases rapidly from 0 - 500 S cm^{-1} when adding 0–1.2 wt % DMSO in the PEDOT:PSS solution and reaches a plateau with additional DMSO. In the spin-cast films, σ increases gradually from 0 - 1000 S cm^{-1} with increasing the DMSO concentration from 0 to 4 wt %. However, the reason for the two different trends of the dependence of σ with DMSO concentration (%wt) is not yet fully

known. One possible reason is the different combinations of evaporation temperature and time used in preparing the drop-cast and spin-cast films, which will alter the molecular-scale kinetics that determines the polymer morphology.

Y. Du et al. ^[56] made a Bi₂Te₃ (NS)/PEDOT:PSS composite film via drop casting technique with 4.1 wt% Bi₂Te₃. This film had an electrical conductivity as high as 1295.21 S cm⁻¹, which proved to be higher than PEDOT:PSS films doped with DMSO. They also found that as the content of Bi₂Te₃ increased from 0 to 4.1 wt%, the electrical conductivity increased in a similar pattern. It was concluded that deposited PEDOT:PSS via electropolymerization on screen-printed platinum electrode surface demonstrates stable charge-discharge profile under water-flow test in comparison to drop cast modified electrodes, although both electrodes maintain charge-discharge stability under static flow condition. FESEM-EDS results reveal that the morphology and elemental composition of PEDOT:PSS film deposited via drop cast method changed drastically after 15 days of storage in PBS, pH 7.1, whereas EPD-modified ones maintained almost the same morphology, charge/discharge CV and elemental chemical composition ^[57]. The results obtained by M. Eslamian et al. ^[58] show a 10x increase in electrical conductivity of PEDOT:PSS films fabricated under substrate vibration-assisted drop-casting (SVADC) compared to the films made by traditional drop-casting method. Furthermore, simple planar PSCs created via SVADC show promising properties and performance, with a power conversion efficiency over 3% for an uncomplicated structure without the use of expensive materials and methods, or even optimizing the method by a huge factor.

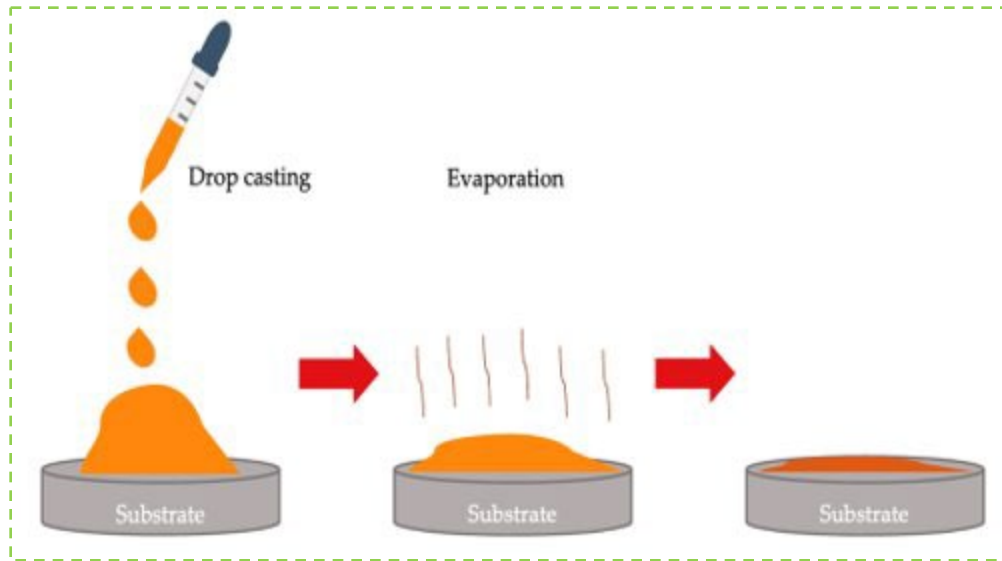


Fig.7 Drop casting method. [4]

2.2 3D printing of PEDOT:PSS

F.M. Kordshuli et al. [3] made use of low power ultrasonic vibrations - both vertical and horizontal - to help increase film uniformity and nanostructure. The method was found quite successful when applied to the pristine PEDOT:PSS solution, where a significant increase in the film conductivity and uniformity was achieved. However, a high-power ultrasonic vibration was found to adversely affect the quality and intactness of the resulting solid film. P.Y. Lin et al. [34] fabricated heterojunction PSCs consisting of a PEDOT:PSS ETL layer that was electrospayed and found that the PCE of this hybrid device was 9.3%. J.H. Lee et al. [35] electrospayed a layer of rGO-PEDOT:PSS onto the pristine separator of Li-S batteries and found that this drastically enhanced the electrochemical performance of the cell due to effective suppression of the polysulfide shuttle effect. In their study, K.C. Hsu et al. [36] used a combination of electrospay and vapor assisted solution technology (VAST) to fabricate PSCs, and their results showed an improved PCE of 10.74%. W. Hwang et al. [37] used the ESD technique

to produce a polymer LED device that exhibited a maximum current efficiency of 24 cd A^{-1} , which is comparable to PLEDs manufactured by spin-coating methods. S.K. Shah et al. [38] fabricated a heterojunction organic solar cell with direct structure (ITO/PEDOT:PSS/P3HT:PCBM/Ca/Al). This device showed a power conversion efficiency of 1.62%, given that the entire device was fabricated using purely electro spray deposition. X.Y. Zhao et al. [39] utilized the electro spray deposition method to fabricate OPV devices, with the addition of acetic acid as a solvent to the precursor solution. These devices showed a PCE of $2.99 \pm 0.88\%$ under AM 1.5 solar simulation, which was found to be at par with the spin coated OPV with the same materials.

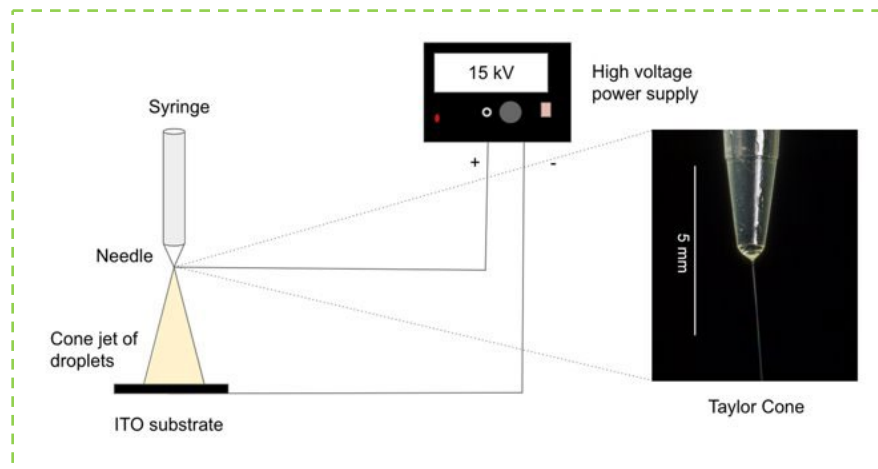


Fig.8 Electro spray deposition technique, with magnification of Taylor cone and jet stream.

2.3 Challenges

Indium tin oxide (ITO) has been widely used as a transparent electrode in optoelectronic devices. However, ITO has several drawbacks, including its high brittleness, which makes it unsuitable for flexible electronic devices. Furthermore, the scarcity of indium and high demand for its compounds has resulted in the

increase of its cost. The ITO components of polymer solar cells comprise a large portion of their overall cost. Additionally, ITO has some inherent problems such as poor transparency on short wavelengths of visible light (400 to 500 nm), a need for high temperature processing, and the potential for oxygen and indium to diffuse into the organic layer. To address these problems, academia and industry are actively investigating new transparent conductive materials to replace ITO. After many years of extensive research in this field, PEDOT:PSS was found out to be the most promising conductive candidate. That being said, PEDOT:PSS naturally has low conductivity ($<1 \text{ S cm}^{-1}$), thereby limiting the performance of perovskite solar cells. PEDOT: PSS aqueous dispersions have low conductivity because the PSS chains are electrically insulating. Several methods have been tested and implemented to improve the conductivity of PEDOT:PSS aqueous solutions, which include adding surfactants, ethylene glycol, glycerol, DMSO and IPA. An increase of about 2 to 3 orders of magnitude were seen in the conductivity of these films, resulting from the methods mentioned above [2].

In addition to the electrical conductivity, poor moisture resistance and high chemical-activity of PEDOT:PSS are other common issues faced by scientists and researchers, which may significantly hamper its applicability, leading to poor stability and reproducibility of the related PSCs [6]. There are a number of common failure mechanisms for slot-die coatings including (i) the 'low-flow' limit, where the breakup of the downstream meniscus causes discontinuity in the wet film (ii) discontinuous film defects such as rivulets, where the coating breaks into multiple smaller stripes with gaps (iii) completely discontinuous films where the coating

stops and starts along the length of the substrate (iv) air-entrainment defects, associated with the breakup of the upstream meniscus leading to 'bubbles' within the wet film and areas of uncoated substrate and (v) 'flooding' or 'dripping' where the flow of ink to the head is too great compared to the coating speed and results in the gradual build-up of ink at the coating head and loss of pre-metering and the expected film thickness ^[9]. PEDOT:PSS is very expensive, thus making it tough to utilize it in large scale PSCs manufacturing. Furthermore, the acidity of this solution aids in etching the ITO layer on which it has to be printed on and degrades the perovskite layer it is in contact with ^[14]. The reported PCE (power conversion efficiency) of OPVs with the e-sprayed PEDOT:PSS top electrode is lower than that with the metal top electrode. The reason for such low PCE could be low conductivity, low reflectivity, interface interaction, etc. ^[23]

2.4 Principle and Methodology

N. Duraisamy et al. ^[18], prior to electro spraying PEDOT:PSS films on plasma treated ITO substrates, analyzed the operating envelope for the prepared PEDOT:PSS solution. According to their findings, varying flow rates and the applied voltage between nozzle and substrate resulted in different modes of spray such as dripping, micro-dripping, unstable jet cone, stable jet cone, and multi-spray jets. Keeping the flow rate constant at 1200 $\mu\text{L/h}$ (20 $\mu\text{L/min}$), the voltages were varied. From 0 to 3.3 kV, natural solution dripping was observed. Just above 3.3 kV and 3.9 kV, micro-dripping of the droplets was seen. Additional increase in the applied voltage resulted in an unstable jet cone from the nozzle to the ITO substrate, which lasted just below 5.4 kV. Between 5.4 kV and 7.1 kV, a stable jet

cone was established. Finally, increasing the voltage beyond 7.1 kV resulted in a multi-jet spray condition. It was also noted that the thickness of the deposited film can be regulated via parameters such as standoff distance, spray time, ink flow rate, concentration of the ink, and substrate velocity. The droplet size is one of the critical factors to be taken into consideration while printing liquid polymers onto substrates via ESD. This is because the film's morphology depends upon the effective drying of the droplets. The equation for the droplet size was proposed by De La Mora and Loscertales [24-25], which is given as follows,

$$d = a_1(\epsilon_r)\left(\frac{1}{K}\right)(Q\epsilon_r\epsilon_0)^{1/3} \quad (5) \quad [24-25]$$

where d is droplet diameter (m), a_1 is a function of the liquid permittivity, Q is liquid flow rate (m^3s^{-1}), ϵ_0 is permittivity of a vacuum ($\text{CV}^{-1} \text{m}^{-1}$), ϵ_r is relative permittivity of the liquid ($\text{CV}^{-1} \text{m}^{-1}$), and K is conductivity (S m^{-1}).

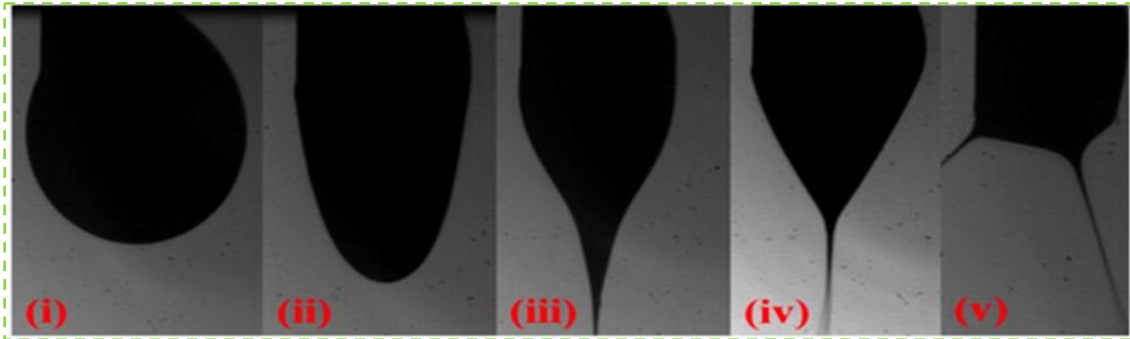


Fig.9 (i) Natural dripping, (ii) Micro-dripping, (iii) Unstable jet cone, (iv) Stable jet cone, (v) multi-jet cone modes of e-spray under varying applied voltage [18].

The degree of solvent evaporation from the droplets as they travel toward the substrate is determined by the ratio of time-of-flight t_f and droplet evaporation time t_e . t_e is approximately proportional to the surface area of the droplet and can be estimated by the d-square law [32],

$$t_e = d^2/K \quad (6) \text{ [32]}$$

where d is the initial diameter of the droplet, and K is the solvent evaporation rate.

For this study, a pre-prepped PEDOT:PSS solution was injected into the nozzle of the syringe via a set of G-codes to move the plunger downwards. This resulted in a small droplet of the polymer solution forming at the tip of the syringe i.e., the exit of the nozzle. Once the high voltage supply was turned on, a strong electric field was generated between the ITO substrate and the exit of the nozzle. Next, a new set of G-codes are entered so that the PEDOT:PSS solution is ejected out of the nozzle, thereby forming small droplets under the influence of the electric field. This is due to the overcoming of surface tension between the droplet and the inner surface of the nozzle exit by the Coulomb force due to the generated electric field. These small droplets are sprayed onto the ITO substrate due to them having opposite electric charges on the copper electrode over which the substrates were placed. A high voltage was applied between the tip of the syringe and the copper electrode.

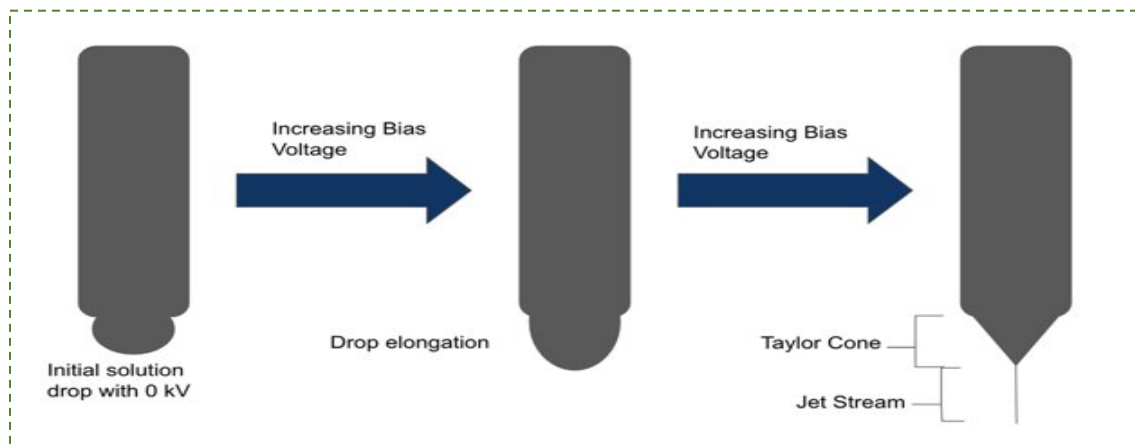


Fig.10 Taylor cone formation and jet stream ejection under influence of electric field.

In Fig.8, we can see that initially, under zero voltage, the droplet is just formed at the nozzle exit, held in place due to the balance between the surface tension between droplet and exit and the weight of the droplet. As we increase the bias voltage, droplet elongation occurs due to the prevalence of the Coulomb force over the gravitational force on the droplet. This stage can be considered as the start of the formation of the Taylor cone. As the voltage is further increased the droplet continues to elongate, and finally, at a certain value, the droplet is ejected out of the exit in the form of a small sphere. A continuous jet stream of PEDOT:PSS droplets is created, which is deposited onto the ITO substrate, thereby resulting in a thin uniform film over the substrate, in the order of nanometers. Ultrasonically induced vibrations were applied to the substrate during and after deposition, in order to increase the uniformity of the film, and decrease the surface roughness, post heat-treatment.

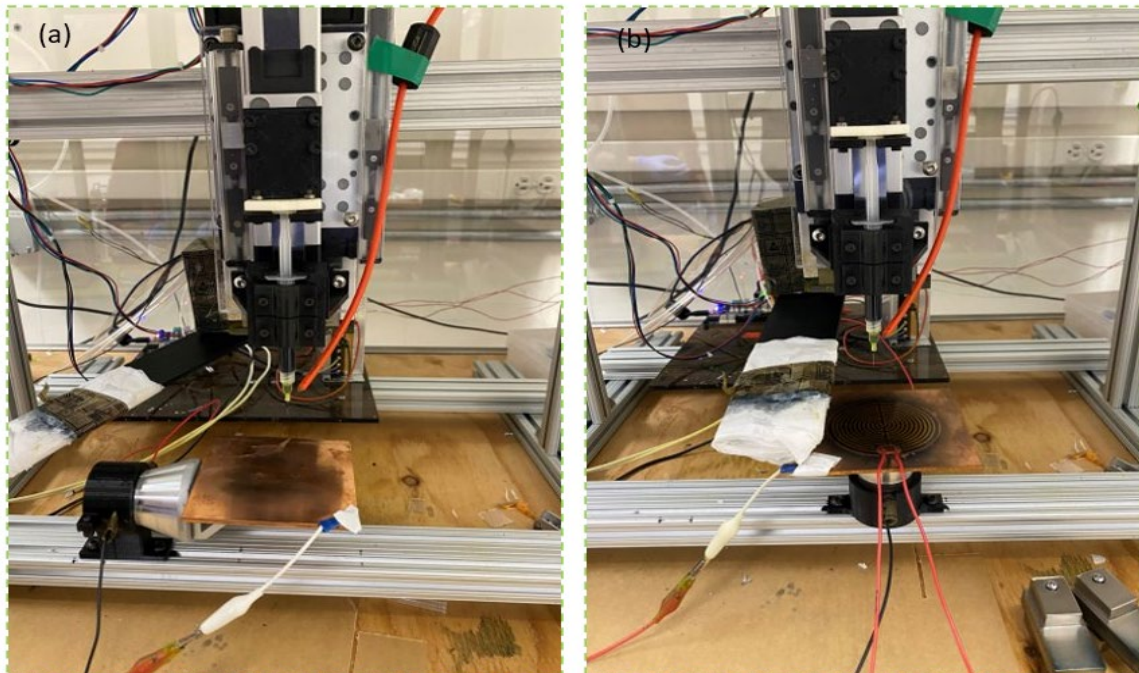


Fig.11 Printing setup with (a) horizontal vibration module, (b) vertical vibration module.

CHAPTER 3 EXPERIMENTAL PROCEDURE

3.1 Materials Selection

AI 4083 PEDOT polymer ink solution (in water) was acquired from Xi'an Polymer Light Corporation. The ink was diluted using DMSO purchased from Sigma Aldrich. The plastic syringes were purchased from BD Medical. The plunger of the syringe was mounted on a mechanical linear actuator with a 40 mm movement range (1 μm resolution, purchased from Parker - Hannifin Corporation) for material extrusion. Stainless steel BSTEAN 32G $\frac{1}{2}$ inch blunt needles (0.09 mm inner dia, 0.25 mm outer dia) used for electrospaying were purchased from Amazon, Inc. Mechanical linear stages for $X/Y/Z$ motions were acquired from Parker-Hannifin Corporation (1 μm resolution, 150 mm movement range). A pair of aluminum plates (purchased from BCAMD) were used to mount on the top of stages which moved in both X and Y directions and served as a printing platform. The $X/Y/Z$ mechanical linear stages, syringe pump stage, and heating pad were all controlled by a Duet 2 control board that was purchased from Filastruder. It also had modules for stepper motor control, heating control and thermocouple reading. A RepRap firmware configuration tool was used in the control system and powered by a 12V 30A DC universal regulated switching power supply that was purchased from Alitove. HV350REG (purchased from Information Unlimited) was used as the high voltage power supply to generate an electrical field for deposition ^[16]. Two sets of Nickel brushed stainless steel clamps were purchased from Amazon Inc website. An acrylic board and epoxy were used to modify the set of clamps.

3.2 PEDOT: PSS Printing Ink Preparation

AI 4083 PEDOT was diluted with 70% IPA (Isopropyl Alcohol) by volume. The solution was then filtered using a 0.45 μm filter to remove the undispersed nanoparticles. The solutions have to invariably be kept in a refrigerated and cool environment if not being used for extended periods of time to avoid degradation of solution properties and evaporation of the solvent. The substrates on which the PEDOT: PSS films were to be printed were cut out from a sheet of ITO glass, cleaned with isopropyl alcohol sprayed Kim wipes and ozoned for 15 minutes.



Fig.12 Prepared PEDOT:PSS solution. (10% PEDOT in 90% IPA v/v)

The clamps were modified by cutting an acrylic board with appropriate dimensions and adhering it to the bottom base of the clamp using epoxy. This was left to cure over 24 hours and was now ready to be used to hold the ITO slides in place during application of ultrasonic vibrations. They were fixed onto the base copper electrode on top of the transducer, which would hold the slides.

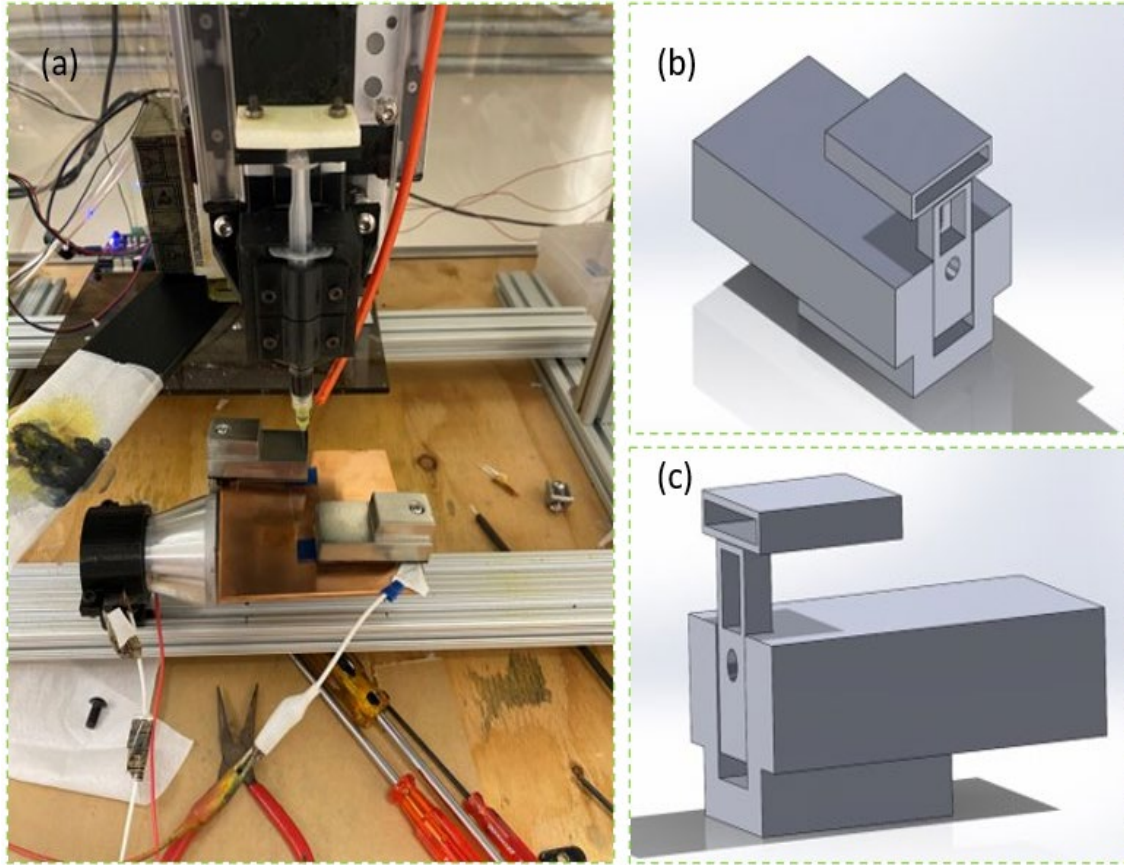


Fig.13 (a) ITO slides held in place using stainless steel clamps, (b) Isometric view of CAD generated clamp, (c) Side-Isometric view of CAD generated clamp.

3.3 Electrically Assisted Direct Ink Deposition with and without Vibration

3.3.1 Electrically Assisted Direct Ink Deposition

For the electrospray deposition of PEDOT: PSS films on the prepared ITO substrates, a 90 μm diameter BSTEAN syringe needle was used. The bias voltage was kept at 12 kV, and the substrate was fixed at a relative distance of 40 mm from the tip of the syringe. The syringe was fitted into the 3D printed holder, and two sets of clamps (3D printed) were used to hold it in place during printing. First, the plunger was moved down by 0.1 mm increment(s) to initialize the process, i.e., to ensure the solution fills in the air gap right above the base of the needle, right up until the point where the droplet first starts forming at the tip of the needle. The

plunger was further moved down the syringe using a set of G codes (G1 U1.2 F2.0), thereby squeezing fine droplets to eject out of the needle. The deposition time was kept at 30 seconds via the pre-set Arduino code for the device. The code controls the shutter which covers the substrate over the top as soon as the time limit is reached.

3.3.2 Electrically Assisted Direct Ink Deposition with Ultrasonic Vibration.

Ultrasonic vibrations (vertical and horizontal) were induced and applied through the electric transducer during deposition. In the initial stages of this research, when vibrations were applied, the ITO substrates that were used seemed to move away from their original position due to increasing amplitude of vibration i.e., increase in current. This will result in the film not being uniform over the substrate, with a few regions not having any deposited PEDOT layer at all. In order to avoid this, the nickel brushed clamps purchased were modified by attaching an appropriately cut acrylic board to the longer base using epoxy. This was done since the minimum clamp depth was not enough to keep the ITO substrates stationary during the application of ultrasonic vibrations. Current through the ultrasonic transducer was adjusted to 0.15 A and 0.26 A before printing. A relay was installed to the ultrasonic generator, and then connected to the Arduino board to control the time after which the ultrasonic vibrations were applied during printing. The Arduino code was adjusted to ensure that the right button moved the shutter away from its original position, and the vibrations were turned on at the time it was designated to. Button 1 (left as shown in Fig.12) will move the shutter away by 85° from the Y axis and come back to its original position

(20° from Y axis) after 30 seconds of deposition. Button 2 (center as shown in Fig.12) will move the shutter away by 85° and turn on the ultrasonic vibrator after 15 seconds of deposition, and switch it off after the next 15 seconds, maintaining the 30 second deposition time. Button 3 (right as shown in Fig.12) will move the shutter to its secondary position as mentioned above and turn on the vibrations at an interval of 5 seconds and 1.5 seconds (after code was adjusted and re-uploaded).

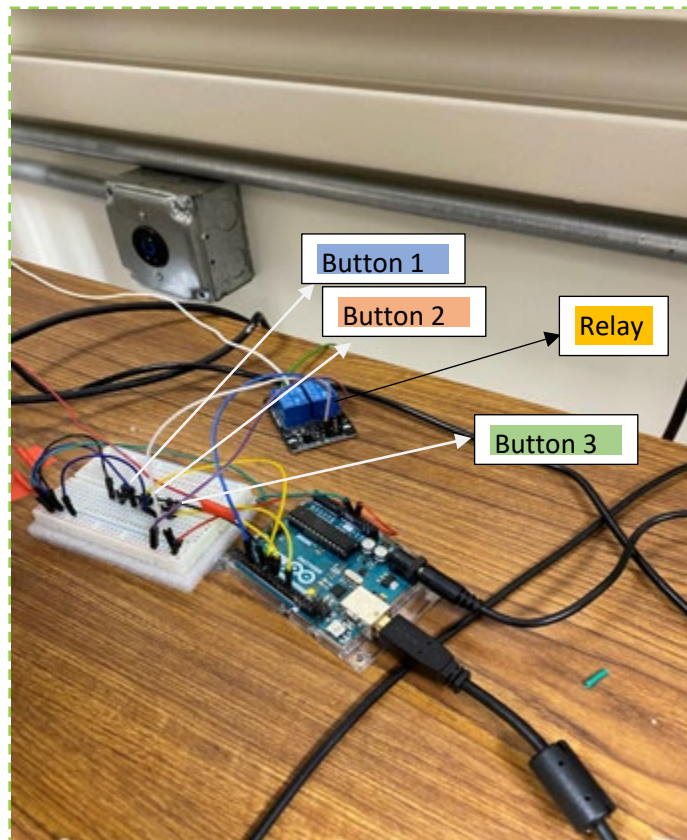


Fig.14 Arduino control board with ultrasonic vibrations generator relay.

3.3.3 Ultrasonic Vibrations after Electrically Assisted Direct Ink Deposition

Vertically and horizontally induced vibrations were applied for 120 seconds after the electrically assisted direct ink deposition. The vertical vibrational setup consisted of an electronic transducer with electrodes attached to the base, two hex

screws and nuts, vertical support, heat pad, connecting wires and copper electrode as cathode. The horizontal vibrational setup consisted of an electronic transducer with electrodes, one hex screw and nut, Gusset bracket, horizontal supports, heat pad, connecting wires, and a copper electrode as the cathode. However, the heat pad was not used in either case since the PEDOT:PSS solution does not require annealing during direct ink deposition to achieve the best film properties. The transducer was shut off immediately after the shutter moved back into its original position. The substrates were now ready to be annealed.

3.4 Post Deposition-Heat Treatment

After the transducer was shut off, the substrates were kept to anneal for 15 mins at 100 °C. The substrates were then stored in a closed environment, ready to be tested to observe and analyze the microstructure of the surface, electrical sheet resistance and surface contact angle of the printed PEDOT:PSS nanofilms. It is important to note that the degradation time of the PEDOT:PSS films is one week post deposition and annealing, so the tests had to be done within 7 days of printing the layers. The device used for annealing the substrates with printed PEDOT:PSS nanofilms was an ALT (American Laboratory Trading) VWR 7"x7" ceramic hot plate stirred, the image of which is shown below.



Fig.15 Printed ITO slides kept for annealing on ALT VWR Ceramic Stirrer.

3.5 Electrical conductivity

The sheet resistance of the printed films was measured using a KLA Tencor Omnimapper four-point probe device at Macro Technology Works (MTW) in ASU Research Park. It utilizes four highly sensitive probes that are part of an auto-mechanical stage that penetrate through the nanofilm. Two outer probes act as electrodes (anode and cathode), thereby forcing current through the length between them, while the inner probes have a voltmeter attached to them, thus measuring the voltage. The sheet resistivity is then calculated by using Ohm's Law: $R = V/I$. The conditions for measuring the sheet resistance were adjusted accordingly using the software that runs on Windows 3.0. The samples were then placed onto the base of the device, near the center since the probe would touch the samples approximately around that region. Once the samples were ready to be tested, the base of the device would lower itself into the chamber, and the probe

would move linearly to the central region and conduct two measurements (as adjusted pre-measurement) over the surface of the films. The mean sheet resistance of was then displayed on the monitor's screen.

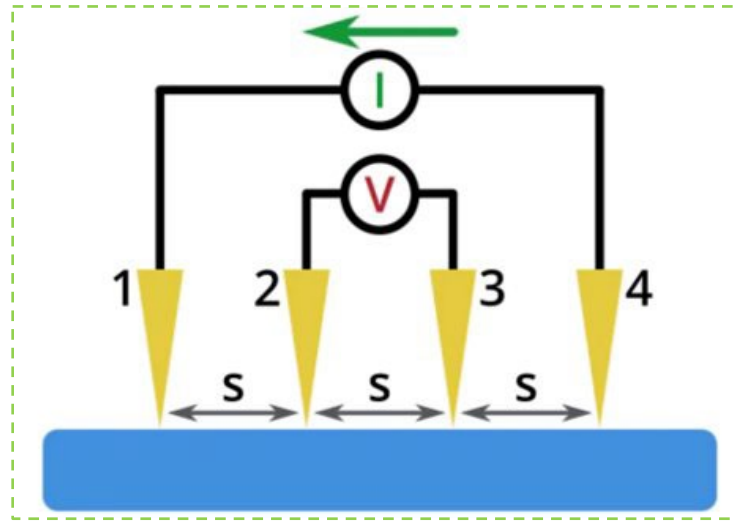


Fig.16 Four-point probe schematic and working ^[45].

The electrical conductivity of the printed films can be calculated from the measured sheet resistances using the equation,

$$\sigma = \frac{1}{Rt} \quad (7)$$

where σ is the electrical conductivity in $S\text{ cm}^{-1}$, R is the sheet resistance of the printed film in $\Omega\text{ sq}^{-1}$, and t is the thickness of the film in μm . From the above equation, it is evident that the electrical conductivity is inversely proportional to the sheet resistance and thickness of the film i.e., larger the sheet resistance and/or thickness, the smaller is the electrical conductivity of the film.

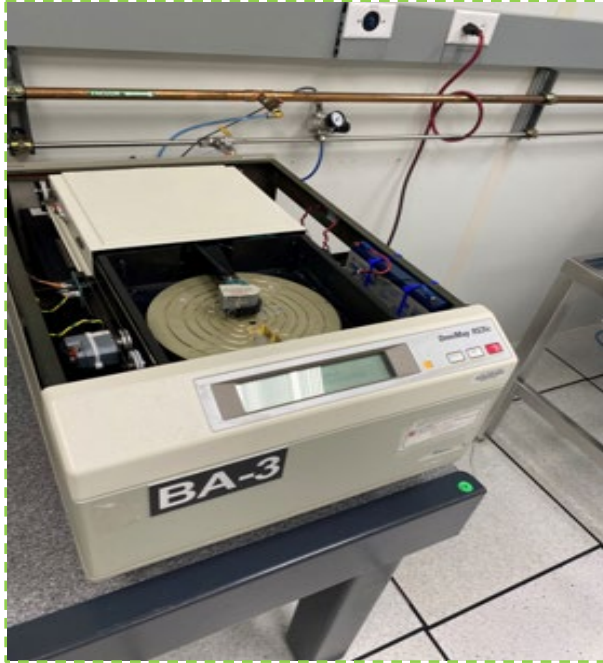


Fig.17 KLA Tencor Omnimap 4-point probe device at MTW.

3.6 Wettability

To understand how characteristics of the liquid affect film behavior during electro spray deposition, we have Young's equation [21],

$$\cos\theta_c = \frac{\gamma_{sv} - \gamma_{sl}}{\gamma} \quad (8) \quad [21]$$

where θ_c is the contact angle of the PEDOT:PSS droplet, γ_{sv} is the interaction between the solid-vapor phase, and γ_{sl} is the interaction between the solid-liquid phase, and γ is the surface tension of the PEDOT:PSS solution. It is evident that the contact angle strongly and inversely depends on the surface tension of the PEDOT:PSS polymer solution, assuming the solid-liquid and solid-vapor phase interactions are constant. A high surface tension implies that there is a high contact

angle, or poor wettability of the PEDOT:PSS solution on the surface of the substrate [21].

There are different methods to reduce the surface tension of PEDOT:PSS liquid solutions, one of them being adding certain surfactants (e.g., Triton-X, TWEEN-20), to the solution. These secondary solvents or surfactants should be miscible with the primary solvent, and compatible with the solute as well. The Marangoni velocity equation shows favorable spreading capabilities of such two-solvent systems, which is given as follows [21],

$$v_{c(x)}^2 = \frac{1}{2\eta(\eta)} \frac{d\gamma}{dx} x(1-x)(-A_l\alpha_l + A_h\alpha_h) \quad (9) \quad [21]$$

where η is the viscosity of the solution, γ is the surface tension, x is the volume fraction of the low surface tension solvent, A_l and A_h are the evaporation velocities, and α_l and α_h are the activity coefficients of the low and high surface tension solvents, respectively [21].

A Sindi contact angle meter was used to measure the surface contact angle of a water droplet on the printed PEDOT:PSS nanofilm. PEDOT:PSS is a hydrophilic polymer, and hence, the smaller the contact angle, the better the film properties. The slides were mounted on a glass cube over the base of the instrument. Light intensity from an LED was adjusted so that the ITO substrates and the block of glass were clearly visible. A syringe containing water was used to wet the surface of the nanofilm with one droplet. A camera mounted on the device was used to click snapshots of the droplet of water. This camera is activated via a

software downloaded onto a laptop. In order to power on the camera, the wire attached was connected to a USB port. Another USB pen drive was used to decrypt the software used to run the camera and conduct the contact angle test. Once the snapshots were taken of the live image, one of them was selected, and automatic fitting operation was performed, from which the resultant contact angle (deg) was calculated and displayed on the screen.



Fig.18 Contact Angle meter ^[59].

CHAPTER 4 RESULTS AND DISCUSSION

4.1 Ultrasonic Vibration Module Construction

4.1.1 Horizontal Vibration Module

A 47065T663_Silver Gusset bracket was adhered to the surface of the top section of the ultrasonic transducer using epoxy. Initially, a hex screw and nut were used to fit the bracket firmly onto the top of the transducer, but the bracket would not hold when the amplitude of the vibrations were increased, causing the surface of the top section of the transducer to wear out a little due to intense friction between the two surfaces, which is why epoxy was used as an adhesive instead. The copper electrode was adhered to the bracket's flat surface using epoxy, over which the heating pad was stuck using some more epoxy. Horizontal supports were attached to the transducer and the setup was kept in a horizontal orientation, with wires connecting the electrodes of the transducer to the power supply. A CAD model of the entire printing assembly with the horizontal vibrational setup was generated on SolidWorks and rendered using Keyshot (refer Fig.19).

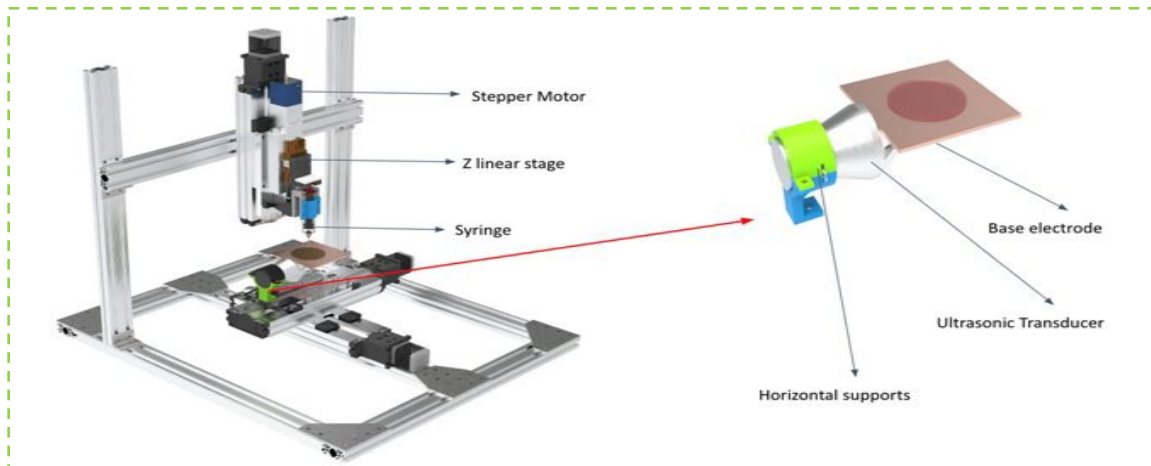


Fig.19 Rendered model of printing setup with horizontally induced ultrasonic vibrations.

4.1.2 Vertical Vibration Module

The copper electrode was adhered to the surface of the top section of the transducer using epoxy, and the heating pad was adhered on top of the electrode using epoxy once again. Vertical supports were attached to the transducer, and the setup was kept in a vertical orientation, with wires connecting the electrodes of the transducer to the power supply. A CAD model of the entire 3D printer with the vertical vibrational setup was generated on SolidWorks, and rendered via Keyshot, the image of which is given below. The vibrational setup was tested prior to attaching it to the 3D printer assembly and without the heating pad by adding a few drops of water to the surface of the electrode, and then varying the current supply (and hence, the amplitude of vibrations). The vibrations seemed to be damped, which could possibly be due to the epoxy acting as an adhesive between the bottom of the electrode and the surface of the top section of the transducer (refer Fig.20).

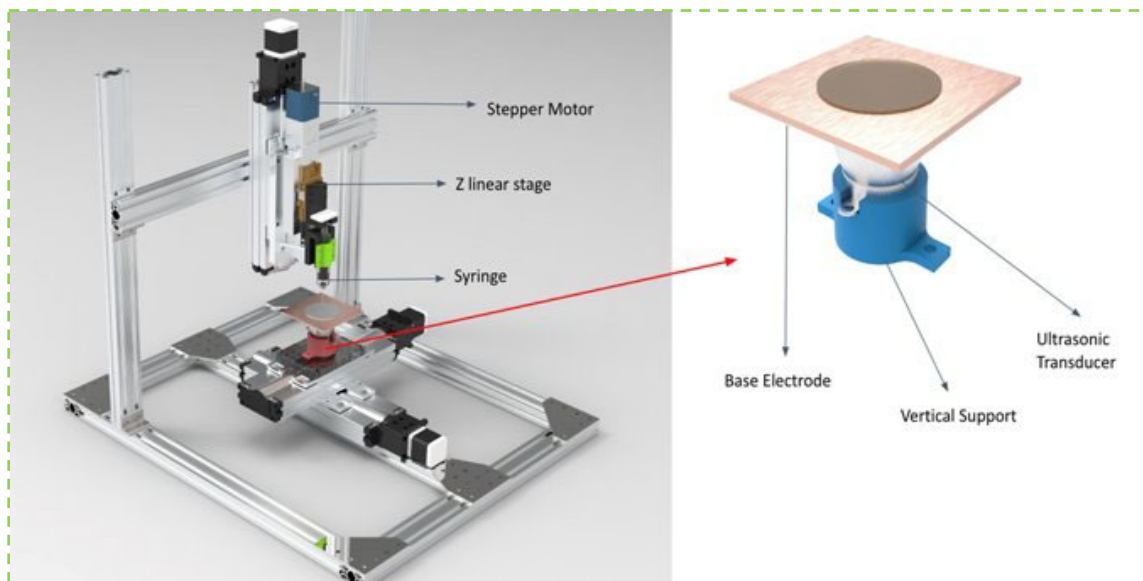


Fig.20 Rendered model of printing setup with vertically induced ultrasonic vibrations.

4.2 Control of Ultrasonic Vibrations

The ultrasonic generator produces vibrations that follow a sine function. These ultrasonic vibrations were controlled by introducing a relay that was attached to the Arduino control board, connecting it to the ultrasonic vibration generator. This relay enable us to introduce intervals of vibrations during printing. An appropriate Arduino code was written for each interval that was to be tested and used during printing. It would be achieved as the relay would turn on the vibrations after the said interval according to the Arduino code for each button (Buttons 2 and 3 in this experiment). For instance, for the 15/15 second interval, the relay would turn on the ultrasonic vibrations from the generator after the first 15 seconds of deposition and switch them off after the next 15 seconds of deposition, thereby completing the deposition cycle. Table.1 has the information that pertains to the intervals and their significance, which is given below.

Interval	Number of Vibration Cycles	Significance
15/15	1	Vibrations turned on during last 15 seconds of printing.
5/5	3	Vibrations turned on during the second, fourth, and sixth 5 second intervals of printing.
1.5/1.5	10	Vibrations turned on during the second, fourth, sixth, eighth, tenth, twelfth, fourteenth, sixteenth, eighteenth and twentieth 1.5 second intervals of printing.

Table 1. Intervals of applied ultrasonic vibrations and their significance.

4.2.1. Connection of Ultrasonic Transducer

The positive electrode of the transducer is connected to the relay, which essentially acts as a switch that breaks the closed circuit during the interval of no vibrations. The relay is controlled by the Arduino control board, and as mentioned previously, the code for each time interval was developed and programmed into their respective buttons. From the relay, another wire is connected to the positive terminal of the ultrasonic wave generator. The negative electrode (anode) of the transducer is connected to the negative terminal of the wave generator. Fig. shows the electrical diagram of the connection to simplify the understanding of the closed-circuit connection.

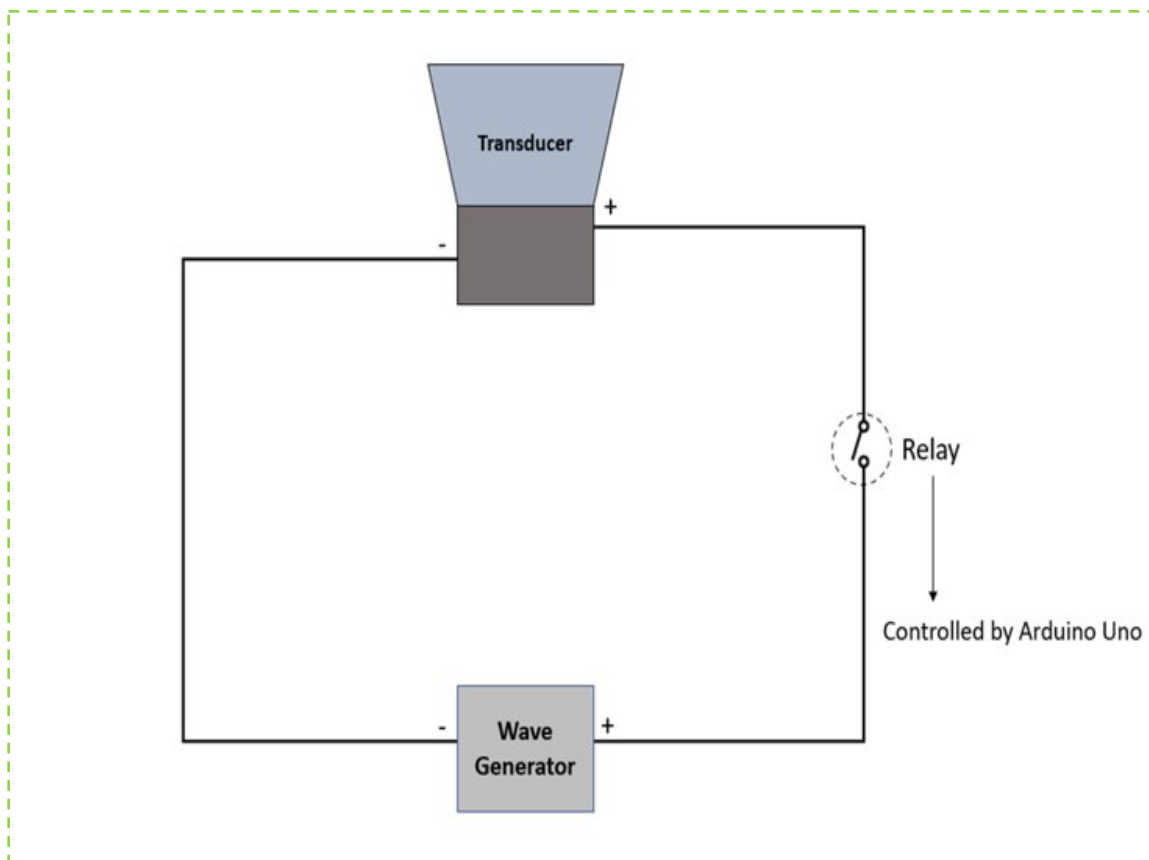


Fig.21 Connection of Transducer, Wave Generator and Relay.

4.2.2. Vibration Regulation

The parameters used for printing are mentioned in Table.2 given below, with their meaning. The relay and Arduino code generated for each parameter were used in conjunction to successfully execute the nanofilm generation and potential effect the vibrations generated would have on the film's properties. The control of the vibrations for the respective intervals has been explained in section 4.2.1.

Parameter	Amplitude of vibration	Interval	Meaning
0.15A, 15/15	0.15 A	15 seconds	Vibrations applied after the first 15 seconds during deposition.
0.15A, 5/5	0.15 A	5 seconds	Vibrations applied after the first 5 seconds during deposition, and switched off during the next 5 seconds, and repeated 2 more times.
0.15A, 1.5/1.5	0.15 A	1.5 seconds	Vibrations applied after the first 1.5 seconds during deposition, and switched off during the next 1.5 seconds, and repeated 9 more times.
0.26A, 15/15	0.26 A	15 seconds	Vibrations applied after the first 15 seconds during deposition.
0.26A, 5/5	0.26 A	5 seconds	Vibrations applied after the

			first 5 seconds during deposition, and switched off during the next 5 seconds, and repeated three times.
0.26A, 1.5/1.5	0.26 A	1.5 seconds	Vibrations applied after the first 1.5 seconds during deposition, and switched off during the next 1.5 seconds, and repeated 9 more times.
0.15A, 30s (D)	0.15 A	30 seconds	Vibrations applied all throughout deposition for 30 seconds.
0.15A, 120s (P)	0.15 A	120 seconds	Vibrations applied for 120 seconds post deposition.
0.26A, 30s (D)	0.26 A	30 seconds	Vibrations applied all throughout deposition for 30 seconds.
0.26A, 120s (P)	0.26 A	120 seconds	Vibrations applied for 120 seconds post deposition.

Table 2. Parameters of printing and their meaning.

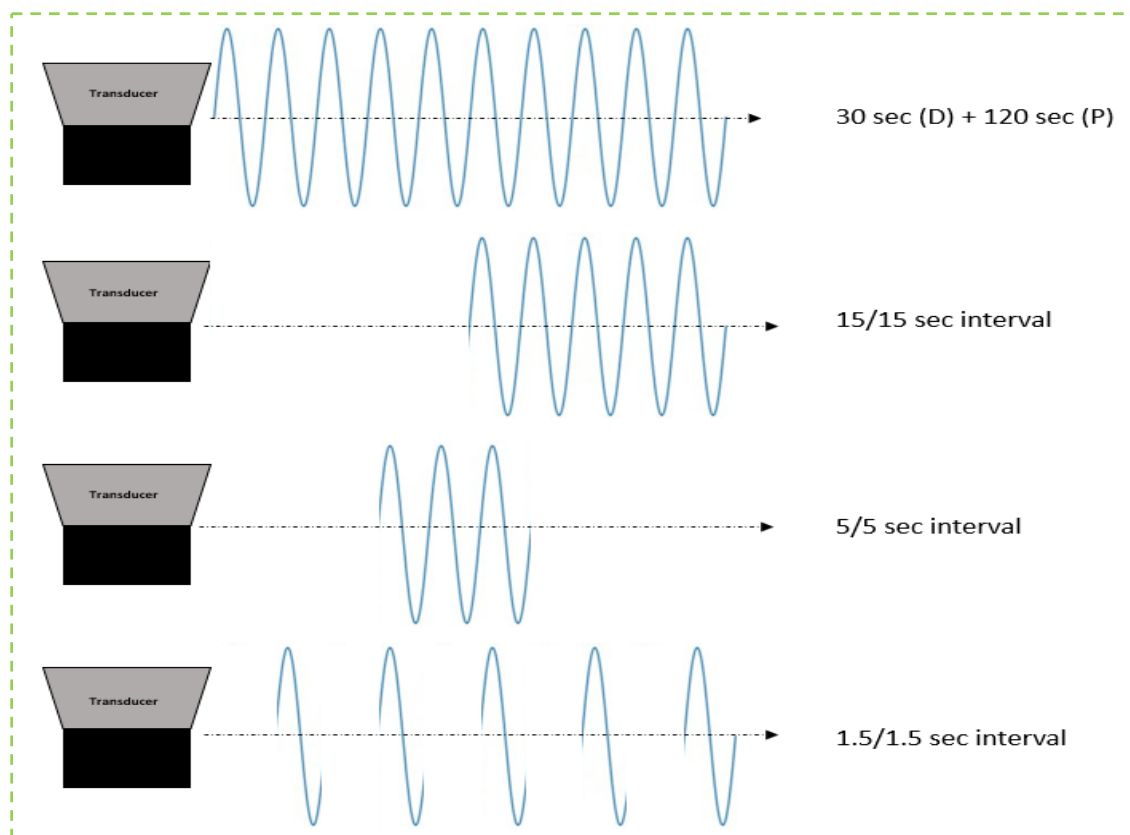


Fig.22 Vibration control via relay.

4.2.3. Potential Influence of Ultrasonic Vibrations

The ultrasonic vibrations were expected to improve the morphology and the uniformity of the nanofilms relative to those printed without any application of vibrations. Applying them during deposition would have a smaller impact on the properties of the film as compared to those applied at intervals. This is because the vibrations applied during the 30 seconds of deposition can potentially cause the PEDOT:PSS nanoparticles to break up into even smaller sized droplets directly upon impact on the substrates, which could cause irregular films being printed.

4.2.3.1 Horizontal

It was thought that the application of horizontal vibrations at certain intervals would allow more time for the droplets to settle down at first upon impact, then

spread out even more over the surface of the substrate with greater uniformity during the intervals when vibrations are applied, and the cycle would thus continue till the deposition was ceased. Since the direction of the applied vibrations is in the XY plane, the results were expected to be relatively better as compared to the ones that would be obtained in the case of vertically applied ultrasonic vibrations. The films generated would be more evenly spread over the surface of the substrates as compared to the case of vertical vibrations.

4.2.3.2 Vertical

Application of vertical ultrasonic vibrations at intervals was thought to prevent the smaller sized droplets generated during breaking of the bigger nano-sized ones directly upon touching the already vibrating surface of the substrates, thereby avoiding evaporation, or bouncing off of the point of impact to possibly land on other sites or regions on the substrates. That being said, it was still expected that fewer number of the nano droplets of the almost settled film would bounce off the surface and land on other regions, or even collide with the successive droplets above the ITO substrates to form bigger ones before finally settling down on the surface. The films generated in this case would be less uniform relative to the case of horizontal ultrasonic vibrations, thereby affecting the results obtained.

Fig.21 shows the potential influence of the application of ultrasonic vibrations in the horizontal and vertical directions as compared to no vibrations.

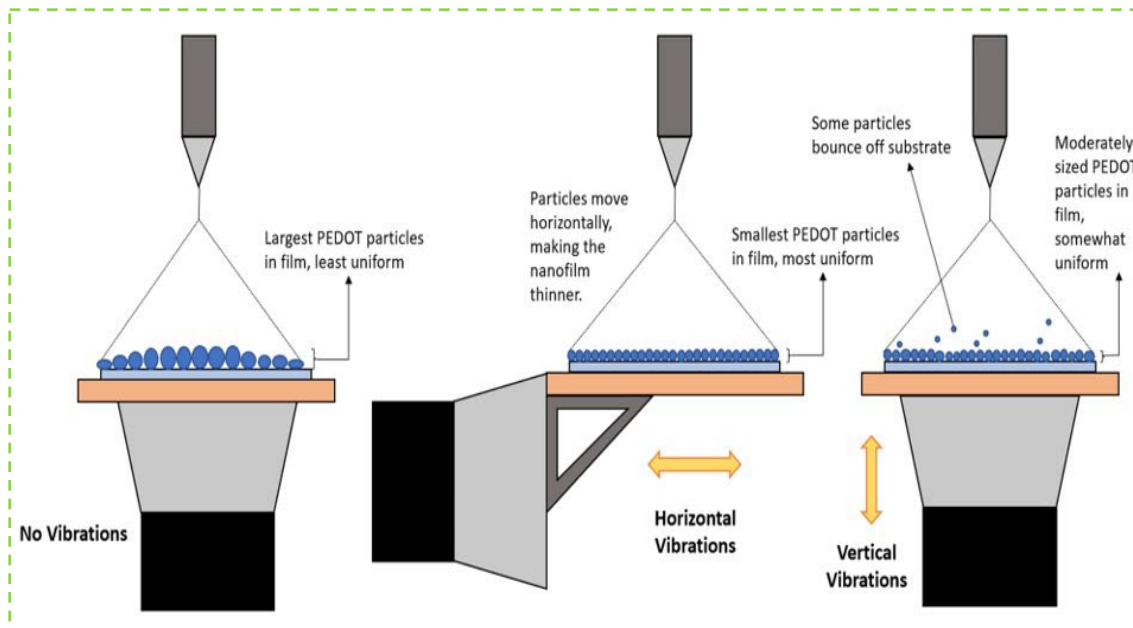


Fig.23 Potential influence of ultrasonic vibrations on the PEDOT:PSS nanofilm.

4.3 Electrical Conductivity

The sheet resistance of the PEDOT:PSS solutions printed with applied ultrasonic vibrations are shown in Fig.19 and Fig.20. The parameters used for printing these slides are noted down in Table.2. The values suggest that the sheet resistance (Ω/sq) are lower for films printed with ultrasonic vibrations have a lower electrical conductivity compared to the ones printed without ultrasonic vibrations for most of the parameters used. The effect of heat generated due to friction between the deposited film and the substrate, however small, cannot be ignored, despite the underlying ITO film being flat and smooth. Additionally, the presence of micro impurities that could have been deposited onto the substrates during or right before printing (during setup) can contribute to the heat generated by increased friction.

4.3.1. 0.15 A Horizontal Vibrations

For the films printed with horizontally applied ultrasonic vibrations of amplitude 0.15 A, the nanofilm printed while vibrations were applied for the entirety of 30 seconds of deposition (0.15A, 30s (D)) seemed to have the least electrical sheet resistance with a value of 87.40 Ω /sq. This is shown in Fig.24 below as the yellow-colored bar. Table.3 summarizes the values obtained with the parameters used in the experiments.

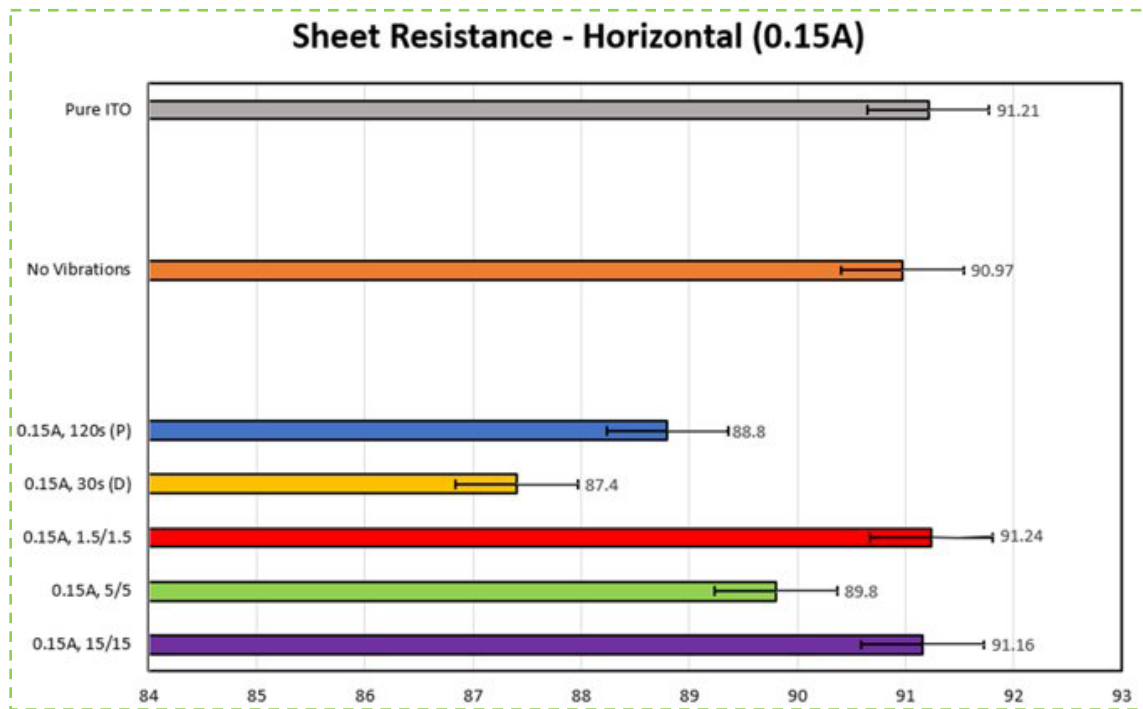


Fig.24 Sheet resistance of films printed with 0.15 A of horizontal ultrasonic vibrations.

Parameter	Sheet Resistance (Ω /sq)
Pure ITO	91.21
No Vibrations	90.97
0.15A, 15/15	91.16

0.15A, 5/5	89.80
0.15A, 1.5/1.5	91.24
0.15A, 30s (D)	87.40
0.15A, 120s (P)	88.80

Table 3. Sheet resistance of films printed with 0.15A of horizontal vibrations.

4.3.2. 0.26 A Horizontal Vibrations

For films printed with horizontally applied vibrations of 0.26 A amplitude through the transducer, the PEDOT:PSS nanofilm with these applied vibrations during the entirety of 30 seconds of deposition (0.26A, 30s (D)) seemed to have the least electrical sheet resistance with a value of 87.26 Ω/\square . This is shown in Fig.25 below as the yellow-colored bar. Table.4 summarizes the various values achieved along with the respective parameters used.

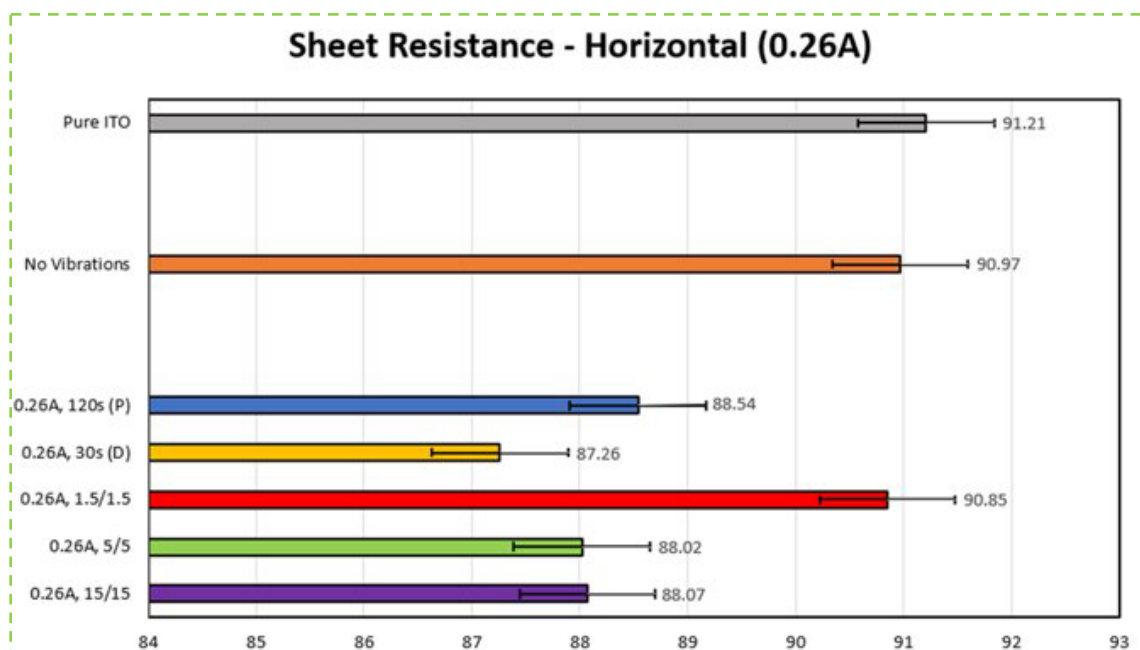


Fig.25 Sheet resistance of films printed with 0.26 A of horizontal ultrasonic vibrations.

Parameter	Sheet Resistance (Ω/sq)
Pure ITO	91.21
No Vibrations	90.97
0.26A, 15/15	88.07
0.26A, 5/5	88.02
0.26A, 1.5/1.5	90.85
0.26A, 30s (D)	87.26
0.26A, 120s (P)	88.54

Table 4. Sheet resistance of films printed with 0.26A of horizontal vibrations.

4.3.3. 0.15 A Vertical Vibrations

For films printed with 0.15 A of vertically applied ultrasonic vibrations, the film printed with these applied vibrations throughout the 30 seconds of PEDOT:PSS deposition seemed to have the least electrical sheet resistance with a value of 87.17 Ω/sq . This is shown as the yellow-colored bar in Fig.26 below.

Table.5 summarizes the various values obtained alongside their parameters.

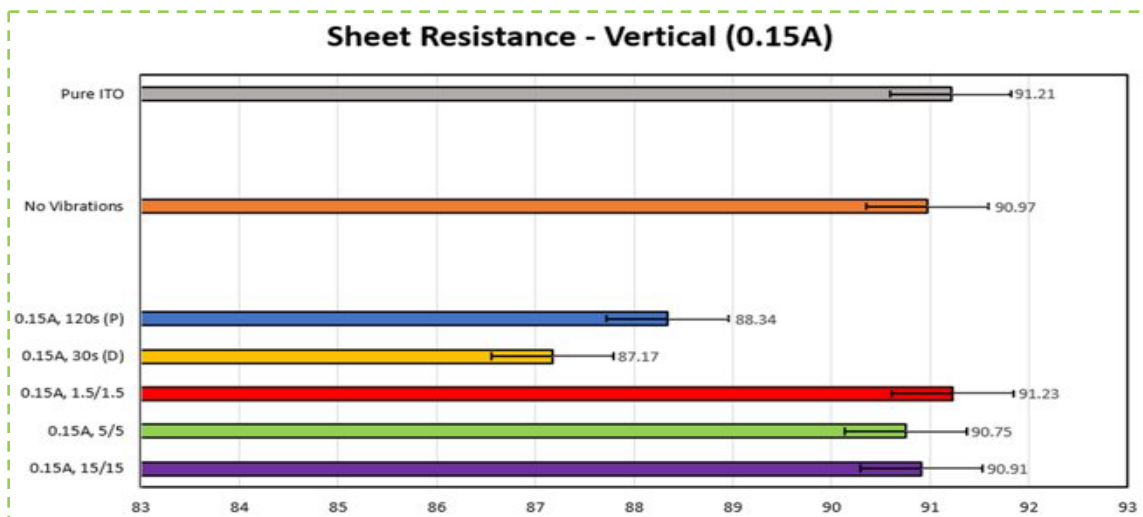


Fig.26 Sheet resistance of films printed with 0.15 A of vertical ultrasonic vibrations.

Parameter	Sheet Resistance (Ω/sq)
Pure ITO	91.21
No Vibrations	90.97
0.15A, 15/15	90.91
0.15A, 5/5	90.75
0.15A, 1.5/1.5	91.23
0.15A, 30s (D)	87.17
0.15A, 120s (P)	88.34

Table 5. Sheet resistance of films printed with 0.15A of vertical vibrations.

4.3.4. 0.26 A Vertical Vibrations

For films printed with 0.26 A of vertical vibrations, the nanofilm printed with an interval of 1.5 seconds seemed to have the least electrical sheet resistance with a value of 86.36 Ω/sq . This is displayed as the light grey-colored bar in Fig.27 below. Table.6 summarizes the values obtained alongside the parameters used.

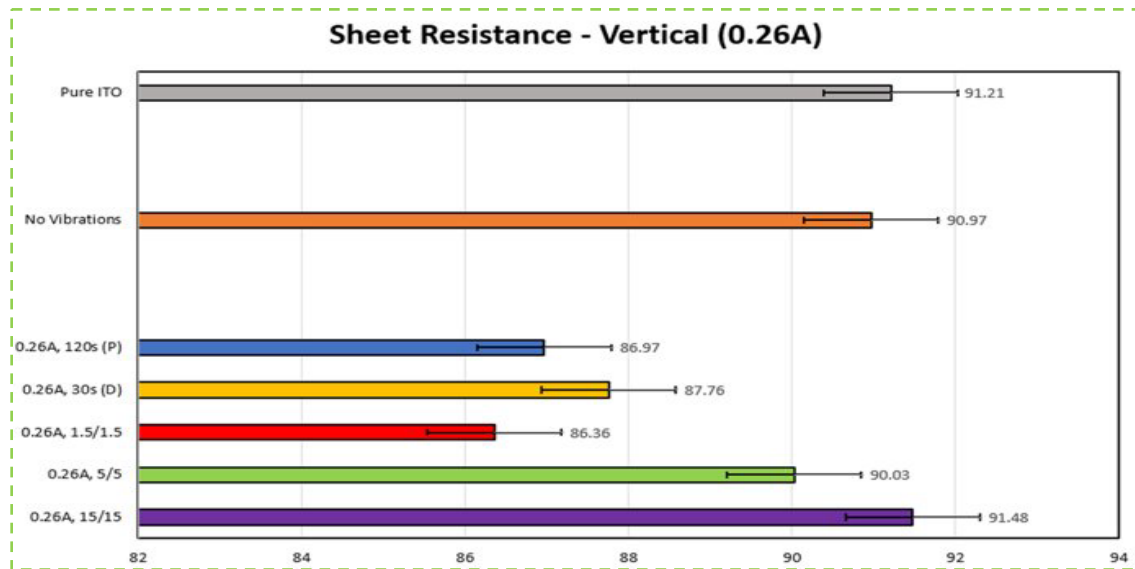


Fig.27 Sheet resistance of films printed with 0.26 A of vertical ultrasonic vibrations.

Parameter	Sheet Resistance (Ω/sq)
Pure ITO	91.21
No Vibrations	90.97
0.26A, 15/15	91.48
0.26A, 5/5	90.03
0.26A, 1.5/1.5	86.36
0.26A, 30s (D)	87.76
0.26A, 120s (P)	86.97

Table 6. Sheet resistance of films printed with 0.26A of vertical vibrations.

From Fig.24-Fig.27 and Table.3-Table.6, we can see that there is a trend that horizontal vibrations applied during 30 seconds of deposition seemed to have the most optimal values of electrical sheet resistance. However, this is not in the case of vertically applied ultrasonic vibrations. The values of pure ITO films were also measured, and they ranged from 87.41-94.24 Ω/sq . In order to confirm if the probes of the 4-point probe instrument were not penetrating the thin nanofilms, electrical sheet resistances of pure glass and films printed with the same parameters on this side of the substrates were measured. Since glass is not electrically conductive, the values obtained for pure glass were displayed as a 'Compliance Limit', and this result was seen in all of the printed slides on this side. It was thus confirmed that the printed nanofilms were too thin ($\sim 10\text{-}30$ nm on an average) thin to accurately measure their respective electrical sheet resistances. Therefore, the electrical 4-point probe instrument cannot be effectively used to measure this value and thus the films' resistivity/conductivity accurately.

4.4 Wettability Evaluation

The contact angle of the printed PEDOT:PSS nanofilms is shown in Fig.21 and Fig.22. From these figures, it can be seen that both horizontally and vertically applied ultrasonic vibrations have a positive influence on the contact angle of the film, thereby decreasing it, relative to pure ITO. PEDOT:PSS is a hydrophilic polymer, hence, lower the contact angle, the better and more uniform the film will be.

4.4.1. 0.15 A Horizontal Vibrations

Relative to the value obtained after testing films printed without any vibrations, for films printed with 0.15 A of horizontally applied ultrasonic vibrations, the lowest value of the contact angle was from the film printed with 15 second interval. The contact angle value of this film is 21.38°. This is shown as the pink bar in Fig.28. Table.7 summarizes the values obtained for the films printed along with their parameters.

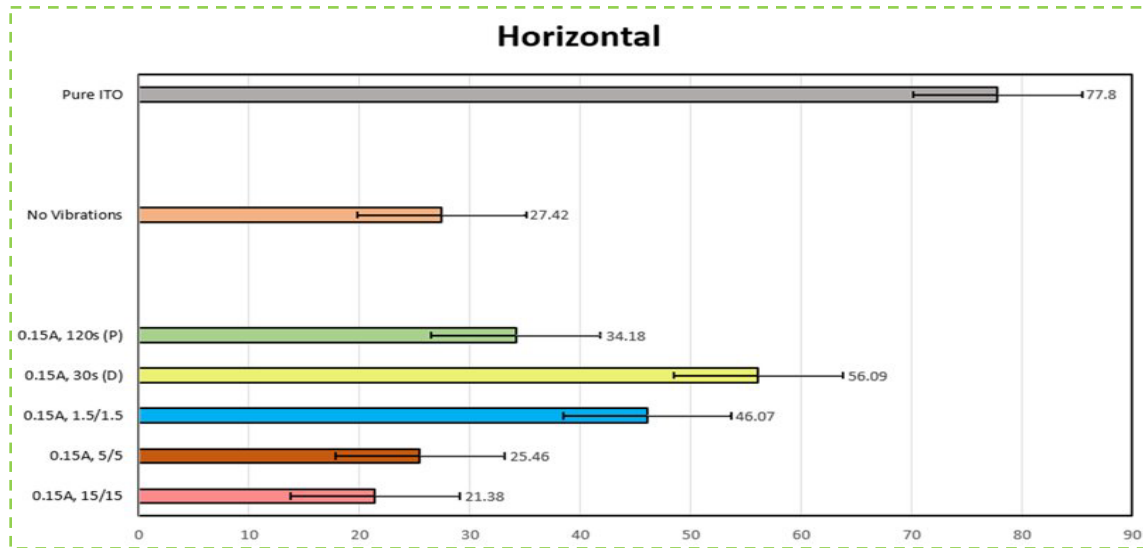


Fig.28 Contact angle of films printed with 0.15 A of horizontal ultrasonic vibrations.

Parameter	Contact Angle (°)
Pure ITO	77.80
No Vibrations	27.42
0.15A, 15/15	21.38
0.15A, 5/5	25.46
0.15A, 1.5/1.5	46.07
0.15A, 30s (D)	56.09
0.15A, 120s (P)	34.18

Table 7. Contact angle of films printed with 0.15A horizontal vibrations.

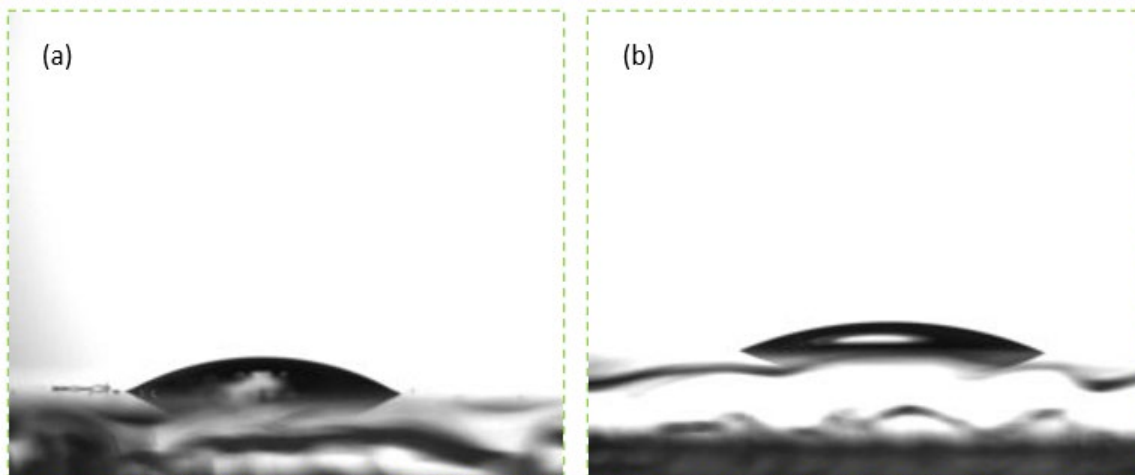


Fig.29 Contact angle of film with (a) no vibrations and (b) 0.15 A, 15/15 s horizontal vibrations.

4.4.2. 0.26A Horizontal Vibrations

While comparing the film printed without vibrations, the films printed with 0.26 A of horizontally applied ultrasonic vibrations during printing, the most optimum value of the contact angle was for the film printed with 1.5 seconds of vibration interval. This is displayed in Fig.30 as the blue colored bar. Table.8 summarizes the values obtained when PEDOT:PSS nanofilms were printed with this amplitude along with their intervals.

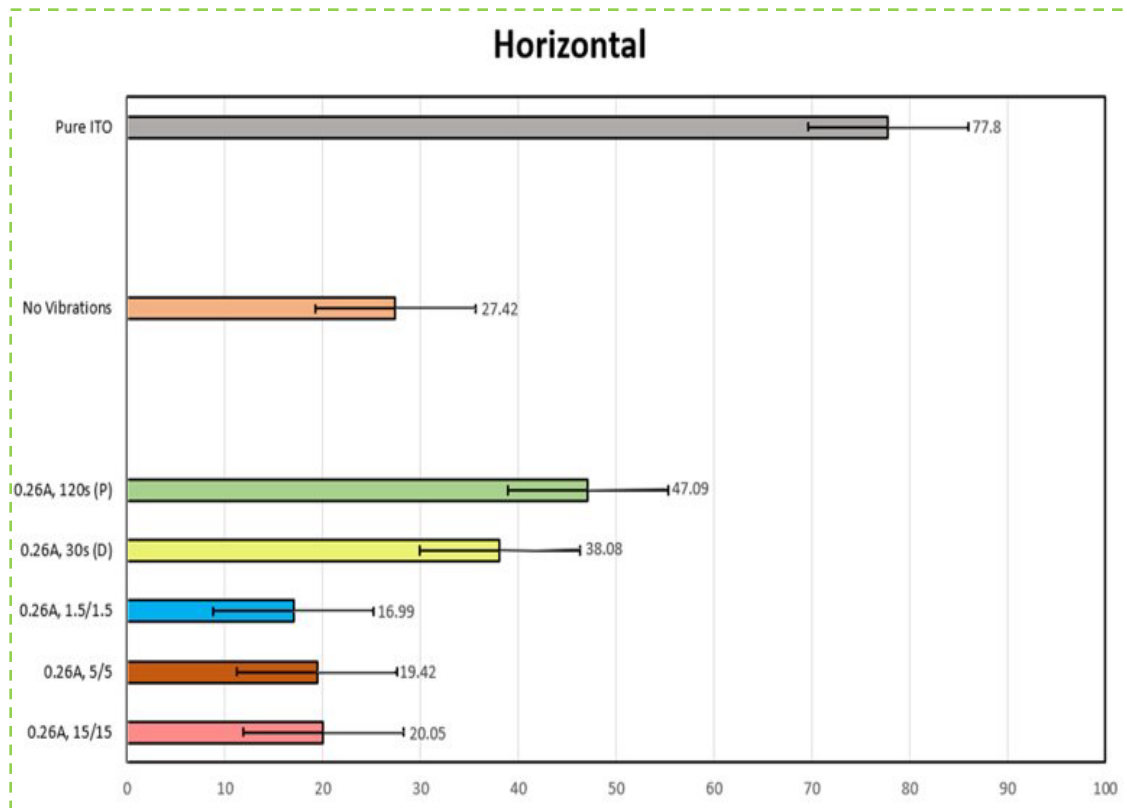


Fig.30 Contact angle of films printed with 0.26 A of horizontal ultrasonic vibrations.

Parameter	Contact Angle (°)
Pure ITO	77.80
No Vibrations	27.42
0.26A, 15/15	20.05
0.26A, 5/5	19.42
0.26A, 1.5/1.5	16.99
0.26A, 30s (D)	38.08
0.26A, 120s (P)	47.09

Table 8. Contact angle of films printed with 0.26A of horizontal vibrations.

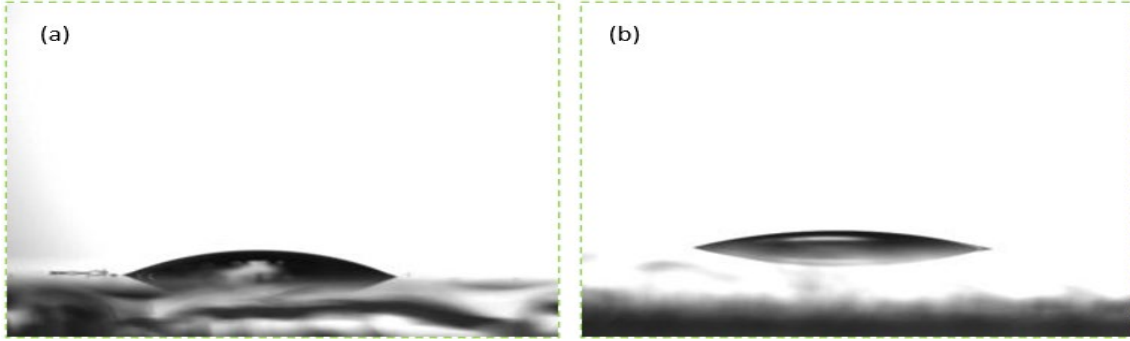


Fig.31 Contact angle of film with (a) no vibrations and (b) 0.26 A, 1.5/1.5 s horizontal vibrations.

4.4.3. 0.15 A Vertical Vibrations

Relative to films printed with no vibrations at all, the least value of the contact angle for films printed with 0.15 A of horizontal vibrations had a value of 18.37° when an interval of 5 seconds of vibrations were applied. This is shown in Fig.32 as the dark orange colored bar, while Table.9 summarizes the values obtained when films were printed with 0.15 A with their respective parameters used during the deposition process.

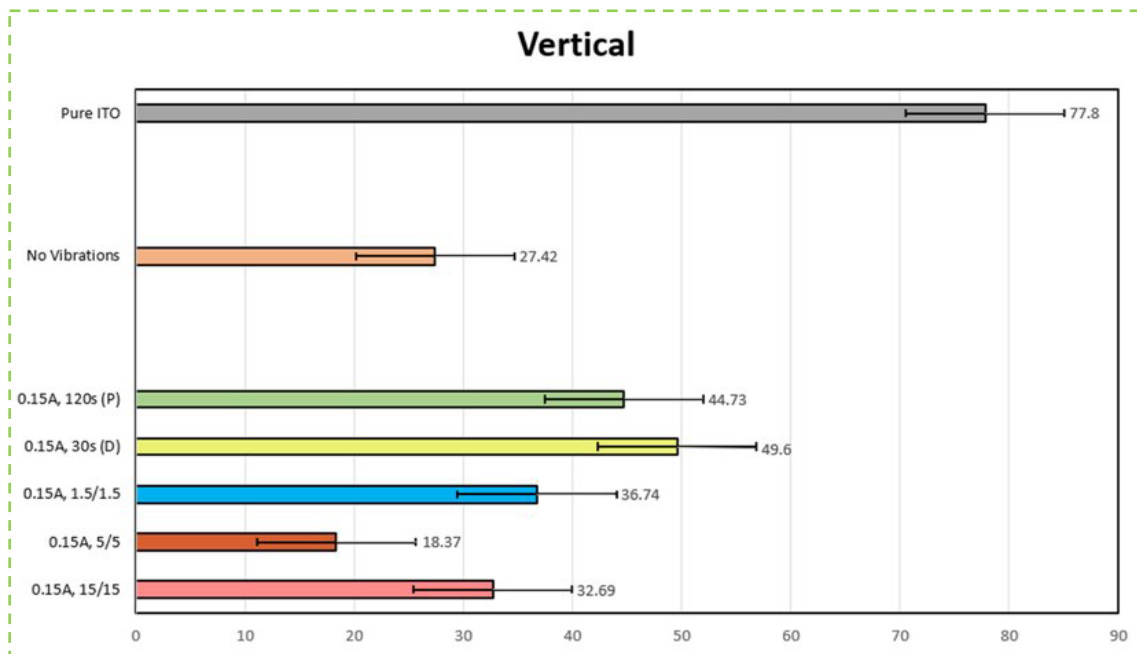


Fig.32 Contact angle of films printed with 0.15 A of vertical ultrasonic vibrations.

Parameter	Contact Angle (°)
Pure ITO	77.80
No Vibrations	27.42
0.15A, 15/15	32.69
0.15A, 5/5	18.37
0.15A, 1.5/1.5	36.74
0.15A, 30s (D)	49.60
0.15A, 120s (P)	44.73

Table 9. Contact angle of films printed with 0.15A of vertical vibrations.

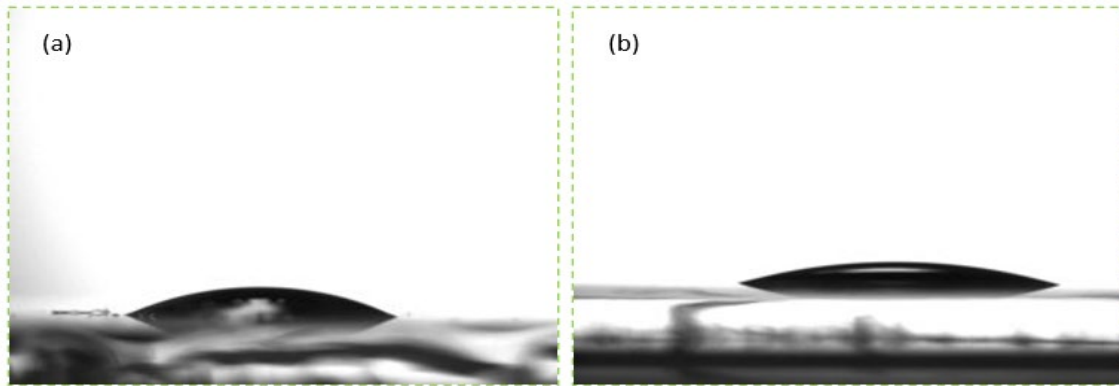


Fig.33 Contact angle of film with (a) no vibrations and (b) 0.15 A, 5/5 s vertical vibrations.

4.4.4. 0.26 A Vertical Vibrations

The film printed with 0.26 A of vertically applied ultrasonic vibrations at an interval of 5 seconds had the lowest contact angle relative to the film printed with no vibrations. The value of this film was observed to be 16.04°. This value corresponds to the dark orange bar in Fig.34. Table.10 summarizes the values obtained when films were printed with this amplitude along with their respective parameters.

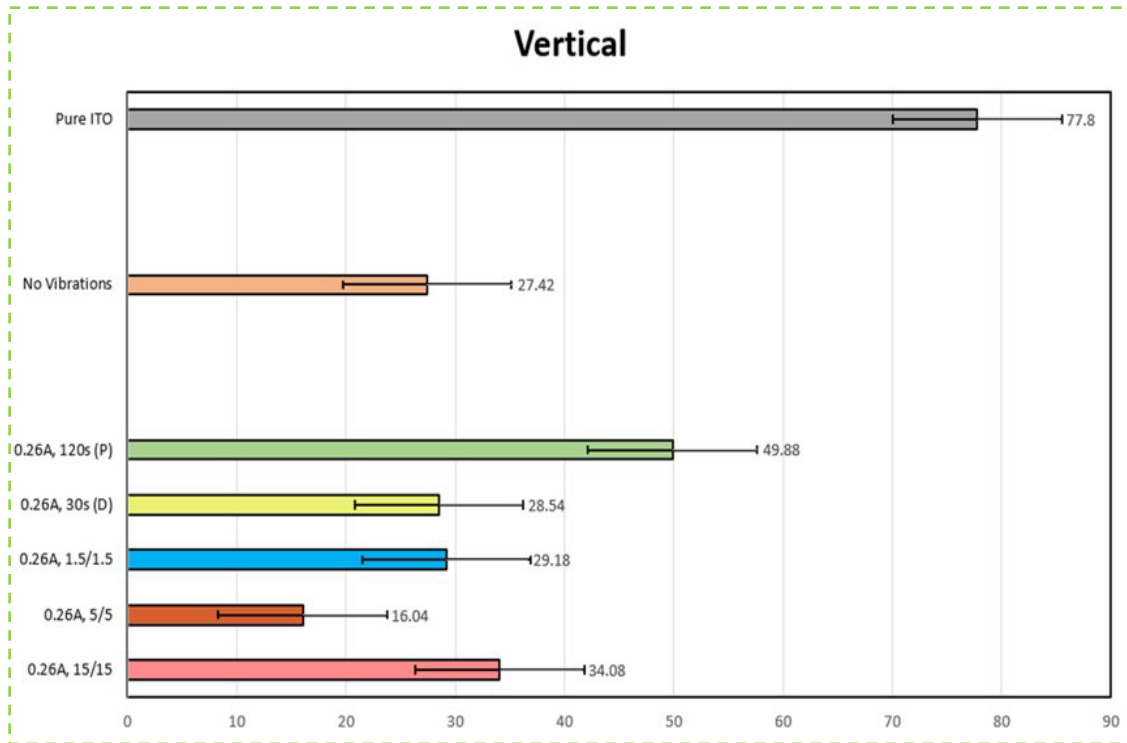


Fig.34 Contact angle of films printed with 0.26 A of vertical ultrasonic vibrations.

Parameter	Contact Angle (°)
Pure ITO	77.80
No Vibrations	27.42
0.26A, 15/15	34.08
0.26A, 5/5	16.04
0.26A, 1.5/1.5	29.18
0.26A, 30s (D)	28.54
0.26A, 120s (P)	49.88

Table 10. Contact angle of films printed with 0.26A of vertical vibrations.

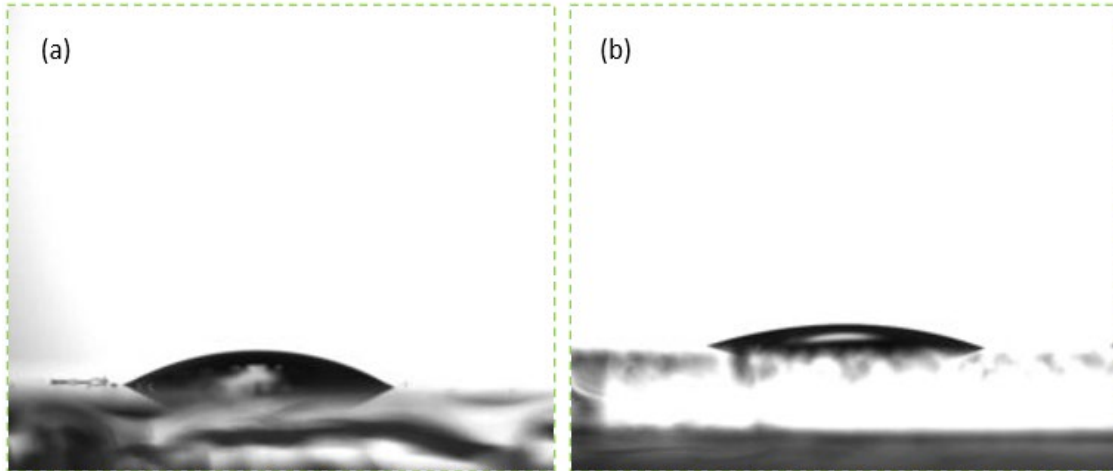


Fig.35 Contact angle of film with (a) no vibrations and (b) 0.26 A, 5/5 s vertical vibrations.

From Fig.28-Fig.34 and Table.7-Table.10, we can see that the lowest contact angle obtained is during 0.26 A of vertically applied ultrasonic vibrations at an interval of 1.5 seconds during deposition. However, a general trend has been observed – horizontally applied vibrations seem to have a more significant impact on the wettability of the film as compared to no vibrations and vertically applied ultrasonic vibrations.

CHAPTER 5 CONCLUSION AND FUTURE WORK

5.1 Summary

In this study, a direct ink deposition technique was utilized with the aid of ultrasonic vibrations to study the effect of these vibrations on the films' properties. A precursor ink consisting of PEDOT:PSS and semiconductor grade IPA (Isopropanol) was printed onto thin ITO substrates with the aid of a high strength electric field as well as the ultrasonic vibrations mentioned above. The properties of the film that were to be evaluated were the electrical sheet resistance and wettability. The sheet resistances obtained are mostly that of the underlying ITO film since the probes of the device were able to pierce the thin nanofilms. The non-uniform deposition was also confirmed due to the contact angle varying at multiple regions over the length of the substrates, some of them showing a variation of more than 10° over the same substrate. However, the contact angle obtained stayed below 90° , thereby proving that deposition was achieved to a considerable extent and that PEDOT:PSS is a hydrophilic organic polymer. It was also shown that horizontally applied ultrasonic vibrations have a more positive impact on the films' property than vertically applied vibrations or no vibrations at all. Only vertical vibrations applied at an interval of 5 seconds each during deposition showed lower values of contact angle relative to no vibrations. This is due to the fact that 5 seconds of pre-deposition and another 5 seconds of deposition during vibrations spread the film more evenly, making it less porous, and giving the ink droplets just the right amount of time to settle down without evaporating or complete drying post

deposition. Additionally, 5 seconds of deposition without vibrations could also avoid the IPA in the ink solution to not evaporate more in ambient environment.

5.2 Future Work

Experiments conducted exhibit that the PEDOT:PSS nanofilm's properties such as morphology, electrical sheet resistance and surface contact angle with water are enhanced with applied ultrasonic vibrations of a certain frequency and duration. However, more work is to be done to fully optimize these films and make them more uniformly distributed along the ITO substrates. This is because even after taking 4-point probe and contact angle measurements of the films over different regions of the ITO substrates, the respective sheet resistance and contact angle values seem to vary over the different regions for most of the substrates over which PEDOT:PSS thin films were printed. That being said, the main objective of this research was to keep our primary focus at or very close to the central region of the substrates. All values mentioned in this work above are from such regions. The sheet resistance of the thin nanofilms cannot be measured using a conventional 4-point probe device and may need to be done using contactless methods such as a non-contact eddy current probe device. Furthermore, new experimental parameters need to be used in order to get more uniform deposition and higher nanofilm thickness, after which it may be possible to use the 4-point probe to measure electrical sheet resistance and then calculate the film conductivity. Atomic Force Microscopy can be used to view topography of the films, and SEM for additional nanostructural characterization. The thickness of such nanofilms can be measured using high precision ellipsometry. PEDOT:PSS films

are primarily used as the HTL in organic solar cells, especially perovskite-based cells. Using electrospray deposition to fabricate such solar cells will aid in reducing wastage of the materials used and shorten its production time as well. Electrospray deposition could probably be used as one of the most effective techniques to mass produce organic solar cells and semiconductor devices in shorter durations as compared to other conventional means that are currently being utilized. In order to ensure that this method is brought to large scale industries, more research is to be conducted on optimizing the process for large-scale production of devices. Adding ultrasonic vibrations to the printing process can help improve the morphology of films, as well as electrical conductivity, thereby resulting in more uniform films with lesser pinholes. This would make the movement of electrons much more efficient through the films, avoiding charge accumulation i.e., higher current densities as observed in non-uniform and rougher films (at peaks and valleys). This will increase the overall power conversion efficiency of the solar cell device and simultaneously avoid damage to it as well.

REFERENCES

- [1] Cheng, T., Zhang, Y. Z., Zhang, J. D., Lai, W. Y., & Huang, W. (2016). High-performance free-standing PEDOT: PSS electrodes for flexible and transparent all-solid-state supercapacitors. *Journal of Materials Chemistry A*, 4(27), 10493-10499.
- [2] Wang, M., Zhou, M., Zhu, L., Li, Q., & Jiang, C. (2016). Enhanced polymer solar cells efficiency by surface coating of the PEDOT: PSS with polar solvent. *Solar Energy*, 129, 175-183.
- [3] Soltani-kordshuli, F., Zabihi, F., & Eslamian, M. (2016). Graphene-doped PEDOT: PSS nanocomposite thin films fabricated by conventional and substrate vibration-assisted spray coating (SVASC). *Engineering Science and Technology, an International Journal*, 19(3), 1216-1223.
- [4] Zabihi, F., Xie, Y., Gao, S., & Eslamian, M. (2015). Morphology, conductivity, and wetting characteristics of PEDOT: PSS thin films deposited by spin and spray coating. *Applied Surface Science*, 338, 163-177.
- [5] Sze, P. W., Lee, K. W., Huang, P. C., Chou, D. W., Kao, B. S., & Huang, C. J. (2017). The investigation of high quality PEDOT: PSS film by multilayer-processing and acid treatment. *Energies*, 10(5), 716.
- [6] Chen, W. H., Qiu, L., Zhang, P., Jiang, P. C., Du, P., Song, L., ... & Ko, F. (2019). Simple fabrication of a highly conductive and passivated PEDOT: PSS film via cryo-controlled quasi-congealing spin-coating for flexible perovskite solar cells. *Journal of Materials Chemistry C*, 7(33), 10247-10256.
- [7] Sahu, N., Parija, B., & Panigrahi, S. (2009). Fundamental understanding and modeling of spin coating process: A review. *Indian Journal of Physics*, 83(4), 493-502.
- [8] Charlot, B., Sassine, G., Garraud, A., Sorli, B., Giani, A., & Combette, P. (2013). Micropatterning PEDOT: PSS layers. *Microsystem technologies*, 19, 895-903.
- [9] Patidar, R., Burkitt, D., Hooper, K., Richards, D., & Watson, T. (2020). Slot-die coating of perovskite solar cells: An overview. *Materials Today Communications*, 22, 100808.
- [10] Whitaker, J. B., Kim, D. H., Larson, B. W., Zhang, F., Berry, J. J., Van Hest, M. F., & Zhu, K. (2018). Scalable slot-die coating of high performance perovskite solar cells. *Sustainable Energy & Fuels*, 2(11), 2442-2449.
- [11] Meng, Q., Jiang, Q., Cai, K., & Chen, L. (2019). Preparation and thermoelectric properties of PEDOT: PSS coated Te nanorod/PEDOT: PSS composite

films. *Organic Electronics*, 64, 79-85.

[12] Tzounis, L., Stergiopoulos, T., Zachariadis, A., Gravalidis, C., Laskarakis, A., & Logothetidis, S. (2017). Perovskite solar cells from small scale spin coating process towards roll-to-roll printing: Optical and morphological studies. *Materials Today: Proceedings*, 4(4), 5082-5089.

[13] Liu, J., Wang, X., Li, D., Coates, N. E., Segalman, R. A., & Cahill, D. G. (2015). Thermal conductivity and elastic constants of PEDOT: PSS with high electrical conductivity. *Macromolecules*, 48(3), 585-591.

[14] Bu, I. Y., Fu, Y. S., Li, J. F., & Guo, T. F. (2017). Large-area electro-spray-deposited nanocrystalline Cu XO hole transport layer for perovskite solar cells. *RSC advances*, 7(74), 46651-46656.

[15] Kim, Y., Lee, J., Kang, H., Kim, G., Kim, N., & Lee, K. (2012). Controlled electro-spray deposition of highly conductive PEDOT: PSS films. *Solar Energy Materials and Solar Cells*, 98, 39-45.

[16] Zhu, Y., Gogoi, B., Alluri, P., Deshpande, M. S., Hutchins, J., Tagbor, E., ... & Li, X. (2022). 3D Printing of Largescale Functional Nanofilm using Electrically assisted Direct Ink Deposition. *Manufacturing Letters*, 33, 744-751.

[17] Shah, S. K., & Gunnella, R. (2020). Efficient method of fabricating polymeric solar cells in multilayered configuration using electro-spray. *Journal of Electronic Materials*, 49, 1794-1800.

[18] Duraisamy, N., Muhammad, N. M., Ali, A., Jo, J., & Choi, K. H. (2012). Characterization of poly (3, 4-ethylenedioxythiophene): poly (styrenesulfonate) thin film deposited through electrohydrodynamic atomization technique. *Materials Letters*, 83, 80-83.

[19] Hiata, T., Ino, T., Ishikawa, R., Ueno, K., & Shirai, H. (2012). Electro-spray-Deposited Poly (3, 4-ethylenedioxythiophene): Poly (styrene sulfonate) for Poly (3-hexylthiophene): Phenyl-C61-Butyric Acid Methyl Ester Photovoltaic Cells. *Japanese Journal of Applied Physics*, 51(10S), 10NE30.

[20] Wei, T. C., Chen, S. H., & Chen, C. Y. (2020). Highly conductive PEDOT: PSS film made with ethylene-glycol addition and heated-stir treatment for enhanced photovoltaic performances. *Materials Chemistry Frontiers*, 4(11), 3302-3309.

[21] Nguyen, T. C., & Choi, W. S. (2022). Investigation of electro-spray-deposited PEDOT: PSS thin film using an electrohydrodynamic jet printer for inverted QLEDs. *Journal of Materials Science: Materials in Electronics*, 1-9.

[22] Tajima, Y., Takaku, H., Hayakawa, H., Okamoto, S., Aoyama, T., & Matsushita, S. (2016). Organic electronic devices fabricated by the electro-spray

deposition method. *Journal of Photopolymer Science and Technology*, 29(2), 301-304.

[23] Lee, H., Park, S., Cho, I. W., Ryu, M. Y., Kang, D., Yi, Y., & Lee, H. (2020). Metal-electrode-free inverted organic photovoltaics using electrospray-deposited PEDOT: PSS and spin-coated HAT-CN exciton blocking layer. *Current Applied Physics*, 20(2), 277-281.

[24] Liao, Y., Fukuda, T., & Kamata, N. (2016). Improved morphology of poly (3, 4-ethylenedioxythiophene): poly (styrenesulfonate) thin films for all-electrospray-coated organic photovoltaic cells. *Advances in Materials Science and Engineering*, 2016.

[25] De La Mora, J. F., & Loscertales, I. G. (1994). The current emitted by highly conducting Taylor cones. *Journal of Fluid Mechanics*, 260, 155-184.

[26] Zuo, C., Bolink, H. J., Han, H., Huang, J., Cahen, D., & Ding, L. (2016). Advances in perovskite solar cells. *Advanced Science*, 3(7), 1500324.

[27] Muradov, A., Frolushkina, D., Samusenkov, V., Zhamanbayeva, G., & Kot, S. (2021). Methods of stability control of perovskite solar cells for high efficiency. *Energies*, 14(10), 2918.

[28] Bishop, J. E., Smith, J. A., & Lidzey, D. G. (2020). Development of spray-coated perovskite solar cells. *ACS Applied Materials & Interfaces*, 12(43), 48237-48245.

[29] Uličná, S., Dou, B., Kim, D. H., Zhu, K., Walls, J. M., Bowers, J. W., & Van Hest, M. F. (2018). Scalable deposition of high-efficiency perovskite solar cells by spray-coating. *ACS Applied Energy Materials*, 1(5), 1853-1857.

[30] Ansari, M. I. H., Qurashi, A., & Nazeeruddin, M. K. (2018). Frontiers, opportunities, and challenges in perovskite solar cells: A critical review. *Journal of Photochemistry and Photobiology C: Photochemistry Reviews*, 35, 1-24.

[31] Kavadiya, S., Niedzwiedzki, D. M., Huang, S., & Biswas, P. (2017). Electrospray-Assisted Fabrication of Moisture-Resistant and Highly Stable Perovskite Solar Cells at Ambient Conditions. *Advanced Energy Materials*, 7(18), 1700210.

[32] Jiang, Y., Wu, C., Li, L., Wang, K., Tao, Z., Gao, F., ... & Deng, W. (2018). All electrospray printed perovskite solar cells. *Nano Energy*, 53, 440-448.

[33] Hameed, M., Mahmood, K., Imran, M., Nawaz, F., & Mehran, M. T. (2019). Co-axial electrospray: a versatile tool to fabricate hybrid electron transporting

materials for high efficiency and stable perovskite photovoltaics. *Nanoscale Advances*, 1(4), 1297-1304.

[34] Lin, P. Y., Chen, Y. Y., Guo, T. F., Fu, Y. S., Lai, L. C., & Lee, C. K. (2017). Electro spray technique in fabricating perovskite-based hybrid solar cells under ambient conditions. *RSC advances*, 7(18), 10985-10991.

[35] Lee, J. H., Kang, J., Kim, S. W., Halim, W., Frey, M. W., & Joo, Y. L. (2018). Effective suppression of the polysulfide shuttle effect in lithium–sulfur batteries by implementing rGO–PEDOT: PSS-coated separators via air-controlled electro spray. *ACS omega*, 3(12), 16465-16471.

[36] Hsu, K. C., Lee, C. H., Guo, T. F., Chen, T. H., Fang, T. H., & Fu, Y. S. (2018). Improvement efficiency of perovskite solar cells by hybrid electro spray and vapor-assisted solution technology. *Organic Electronics*, 57, 221-225.

[37] Hwang, W., Xin, G., Cho, M., Cho, S. M., & Chae, H. (2012). Electro spray deposition of polymer thin films for organic light-emitting diodes. *Nanoscale Research Letters*, 7(1), 1-7.

[38] Shah, S. K. (2020). Fabrication of bulk heterojunction organic solar cells with different configurations using electro spray. *Nano Express*, 1(2), 020037.

[39] Zhao, X. Y., Wang, X., Lim, S. L., Qi, D., Wang, R., Gao, Z., ... & Deng, W. (2014). Enhancement of the performance of organic solar cells by electro spray deposition with optimal solvent system. *Solar Energy Materials and Solar Cells*, 121, 119-125.

[40] Li, J. F., Zhao, C., Zhang, H., Tong, J. F., Zhang, P., Yang, C. Y., ... & Fan, D. W. (2015). Improving the performance of perovskite solar cells with glycerol-doped PEDOT: PSS buffer layer. *Chinese Physics B*, 25(2), 028402.

[41] Tait, J. G., Worfolk, B. J., Maloney, S. A., Hauger, T. C., Elias, A. L., Buriak, J. M., & Harris, K. D. (2013). Spray coated high-conductivity PEDOT: PSS transparent electrodes for stretchable and mechanically-robust organic solar cells. *Solar Energy Materials and Solar Cells*, 110, 98-106.

[42] <https://www.ossila.com/en-us/pages/spin-coating> (accessed 25 Jan, 2023)

[43] Subbiah, A. S., Isikgor, F. H., Howells, C. T., De Bastiani, M., Liu, J., Aydin, E., ... & De Wolf, S. (2020). High-performance perovskite single-junction and textured perovskite/silicon tandem solar cells via slot-die-coating. *ACS Energy Letters*, 5(9), 3034-3040.

[44] Bormashenko, E., Bormashenko, Y., & Frenkel, M. (2019). Formation of hierarchical porous films with breath-figures self-assembly performed on oil-lubricated substrates. *Materials*, 12(18), 3051.

[45] <https://www.ossila.com/en-us/pages/sheet-resistance-theory> (accessed 19 Feb, 2023)

[46] Gong, F., Meng, C., He, J., & Dong, X. (2018). Fabrication of highly conductive and multifunctional polyester fabrics by spray-coating with PEDOT: PSS solutions. *Progress in Organic Coatings*, 121, 89-96.

[47] Wu, X., Li, F., Wu, W., & Guo, T. (2014). Flexible organic light emitting diodes based on double-layered graphene/PEDOT: PSS conductive film formed by spray-coating. *Vacuum*, 101, 53-56.

[48] Zabihi, F., & Eslamian, M. (2015). Substrate vibration-assisted spray coating (SVASC): significant improvement in nano-structure, uniformity, and conductivity of PEDOT: PSS thin films for organic solar cells. *Journal of Coatings Technology and Research*, 12, 711-719.

[49] Bae, E. J., Kang, Y. H., Jang, K.-S., Lee, C., & Cho, S. Y. (2016). Solution synthesis of telluride-based nano-barbell structures coated with PEDOT:PSS for spray-printed thermoelectric generators [10.1039/C5NR07032E]. *Nanoscale*, 8(21), 10885-10890.

[50] Zhi-Hui, F., Yan-Bing, H., Quan-Min, S., Li-Fang, Q., Yan, L., Lei, Z., ... & Rui-Dong, X. (2010). Polymer solar cells based on a PEDOT: PSS layer spin-coated under the action of an electric field. *Chinese Physics B*, 19(3), 038601.

[51] Kim, B. J., Han, S. H., & Park, J. S. (2015). Properties of CNTs coated by PEDOT: PSS films via spin-coating and electrophoretic deposition methods for flexible transparent electrodes. *Surface and Coatings Technology*, 271, 22-26.

[52] Huang, J., Miller, P. F., de Mello, J. C., de Mello, A. J., & Bradley, D. D. (2003). Influence of thermal treatment on the conductivity and morphology of PEDOT/PSS films. *Synthetic Metals*, 139(3), 569-572.

[53] Kim, G. E., Shin, D. K., Lee, J. Y., & Park, J. (2019). Effect of surface morphology of slot-die heads on roll-to-roll coatings of fine PEDOT: PSS stripes. *Organic Electronics*, 66, 116-125.

[54] Parsekian, A. W., & Harris, T. A. (2019). Scalable, Alternating Narrow Stripes of Polyvinyl Alcohol Support and Unmodified PEDOT: PSS with Maintained Conductivity Using a Single-Step Slot Die Coating Approach. *ACS applied materials & interfaces*, 12(3), 3736-3745.

- [55] Colella, M., Griffin, J., Kingsley, J., Scarratt, N., Luszczynska, B., & Ulanski, J. (2019). Slot-die coating of double polymer layers for the fabrication of organic light emitting diodes. *Micromachines*, 10(1), 53.
- [56] Du, Y., Cai, K. F., Chen, S., Cizek, P., & Lin, T. (2014). Facile preparation and thermoelectric properties of Bi₂Te₃ based alloy nanosheet/PEDOT: PSS composite films. *ACS applied materials & interfaces*, 6(8), 5735-5743.
- [57] Benoudjit, A., Bader, M. M., & Salim, W. W. A. W. (2018). Study of electropolymerized PEDOT: PSS transducers for application as electrochemical sensors in aqueous media. *Sensing and bio-sensing research*, 17, 18-24.
- [58] Eslamian, M., & Zabihi, F. (2015). Ultrasonic substrate vibration-assisted drop casting (SVADC) for the fabrication of photovoltaic solar cell arrays and thin-film devices. *Nanoscale research letters*, 10(1), 462.
- [59] https://www.sindin.com/en/Product/info_itemid_413.html (accessed 04 Apr, 2023)
- [60] Eslamian, M. (2017). Excitation by acoustic vibration as an effective tool for improving the characteristics of the solution-processed coatings and thin films. *Progress in Organic Coatings*, 113, 60-73.